

Direct and semi-direct aerosol effects in the NASA GEOS-5 AGCM: aerosol-climate interactions due to prognostic versus prescribed aerosols

C. A. Randles,^{1,2} P. R. Colarco,² and A. da Silva³

Received 2 July 2012; revised 31 October 2012; accepted 1 November 2012; published 16 January 2013.

[1] The present-day climate response to aerosol direct and semi-direct effects is investigated using the NASA Goddard Earth Observing System version 5 (GEOS-5) atmospheric general circulation model. We focus our investigation on aerosol-climate interactions by using either prognostic aerosols from an online aerosol module or aerosols from a climatology based on the prognostic aerosols. As found in previous studies, forcing from all aerosols cools the land surface, warms the troposphere, and impacts global mean circulation, affecting both the strength of the Hadley cell and the zonal mean wind. Less absorbing natural aerosol alone tends to have weaker impacts on global climate. We find that removing the feedback of meteorology on aerosol distributions can significantly impact the climate response depending on the parameter, region, and season considered. Much of the differing climate response to prognostic and prescribed aerosols occurs in regions remote from direct aerosol forcing, such as in the stratosphere and the northern and southern high latitudes. This suggests that aerosol-climate interactions may induce remote dynamical responses to aerosol forcing in global models. The largest effect of removing coupling is to enhance the aerosol optical depth globally over the oceans. This enhancement is due to the removal of the co-variability between aerosol mass and relative humidity on sub-monthly timescales in the high humidity oceanic environment.

Citation: Randles, C. A., P. R. Colarco, and A. da Silva (2013), Direct and semi-direct aerosol effects in the NASA GEOS-5 AGCM: aerosol-climate interactions due to prognostic versus prescribed aerosols, *J. Geophys. Res. Atmos.*, 118, 149–169, doi:10.1029/2012JD018388.

1. Introduction

[2] Aerosols affect climate in several ways. The aerosol direct effect, caused by scattering and absorption of radiation, alters the energy distribution in the atmospheric column. Purely scattering aerosols, such as sulfate and sea salt, radiatively cool the Earth's climate, both at the surface and the top of the atmosphere (TOA). Absorbing aerosols, such as black carbon (BC) and dust, cause radiative cooling at the surface but also warm the atmosphere [Ramanathan and Carmichael, 2008]. At the TOA, the direct effect of absorbing aerosols can be positive (radiative warming) or negative (radiative cooling), depending on the brightness of the surface or clouds lying beneath them [Chýlek and Coakley, 1974]. Tropospheric aerosols may also serve as

cloud condensation nuclei, having a generally cooling indirect effect on climate by modifying cloud reflectivity and lifetime [Charlson *et al.*, 1992].

[3] Absorbing aerosols have a thermodynamic effect on clouds called the semi-direct effect (SDE) [e.g. Hansen *et al.*, 1997]. The semi-direct effect is generally explained as follows: Absorbing aerosols radiatively heat the atmosphere by absorbing shortwave radiation. This heating increases the saturation water vapor pressure, reducing ambient relative humidity (RH) and increasing low-level stability. These effects act to reduce convective cloud formation. The removal of reflective clouds from the climate system then contributes to a net radiative warming effect. However, both observational and modeling studies of the SDE show there is no consensus on the overall sign of the SDE, let alone its magnitude [see Koch and del Genio, 2010 for a thorough review]. For example, observation-based studies of biomass burning aerosol semi-direct effects over the Amazon [Koren *et al.*, 2004] and off the coast of California [Brioude *et al.*, 2009] have shown suppressed cumulus clouds (positive, warming SDE) and enhanced marine stratocumulus clouds (negative, cooling SDE), respectively. Inconsistencies in the sign of the SDE extend to modeling studies, showing up in both general circulation models (GCMs) [e.g. Lohmann and Feichter, 2001; Wang, 2004; Randles and Ramaswamy, 2008; Allen and Sherwood,

All Supporting Information may be found in the online version of this article.

¹GESTAR/Morgan State University, Baltimore, Maryland, USA.

²NASA Goddard Space Flight Center, Atmospheric Chemistry and Dynamics Lab, Greenbelt, Maryland, USA.

³NASA Goddard Space Flight Center, Global Modeling and Assimilation Office, Greenbelt, Maryland, USA.

Corresponding author: C. A. Randles, GESTAR/Morgan State University, Baltimore, Maryland, USA. (Cynthia.A.Randles@nasa.gov)

©2012. American Geophysical Union. All Rights Reserved.
2169-897X/13/2012JD018388

2010; *Randles and Ramaswamy*, 2010; *Perlwitz and Miller*, 2010] and Large Eddy Simulations/Cloud Resolving Model (LES/CRM) studies [e.g. *Ackerman et al.*, 1995; *Johnson et al.*, 2004]. LES/CRM studies simulate larger SDEs than GCMs; however, these models sample different time- and spatial- scales than GCMs and do not include large-scale circulation changes that arise in response to aerosol forcing.

[4] GCM simulations of the present-day direct and semi-direct impacts of aerosols have taken two different approaches. In the first approach, aerosol forcing, optical properties, or dry aerosol mass distributions are prescribed, either derived from observations [e.g. *Menon et al.*, 2002; *Allen and Sherwood*, 2010] or simulated off-line in a chemical transport model (CTM) [e.g. *Sakaeda et al.*, 2011]. The advantage of this approach is that care can be taken to ensure that prescribed aerosol properties give approximate agreement with observations. An example of this would be to force a model with a product produced through assimilation of satellite-derived aerosol optical depth. In addition, for long climate simulations, this step-wise approach is typically less computationally expensive. The disadvantages of this method are that (1) aerosol properties (either dry mass distributions or, less commonly, optical properties or forcing) are typically prescribed on a monthly-mean, inter-annual, or even decadal basis, thus removing any variability in aerosol properties on shorter time-scales, and (2) the distribution of the aerosol properties in both the horizontal and vertical may be inconsistent with the underlying meteorology of the GCM that is responding to their associated forcing. Further, if aerosol forcing, rather than aerosol dry mass distributions, is prescribed the implicit aerosol hygroscopic growth may be inconsistent with the hydrology of the host GCM. This suggests a second approach, increasingly common, in which GCMs include prognostic aerosol schemes. These online aerosol modules vary considerably in their complexity from schemes that track dry aerosol mass to modal and sectional schemes that track both aerosol mass and number. Aerosol transport processes in all of these schemes generally include advection, diffusion, sulfur chemistry, wet and dry deposition, and gravitational settling; more advanced schemes include aerosol microphysical processes such as coagulation. In these online schemes, aerosol distributions (and thus forcing) vary from time step to time step and are internally consistent with the meteorology and hydrology of the underlying GCM. Some major disadvantages of using these online aerosol schemes is that they can be computationally expensive and require careful tuning of the aerosol module so that simulated aerosol optical properties are similar to observations.

[5] Here we consider the direct and semi-direct impacts of aerosols on climate using the NASA Goddard Earth Observing System version 5 (GEOS-5) atmospheric general circulation model (AGCM) forced by observed sea surface temperatures (SSTs). We present a series of experiments designed to examine differences in the climate response to aerosol forcing when aerosols are coupled to the GCM through a prognostic scheme versus prescribed from a consistent monthly-mean climatology of dry aerosol mass mixing ratios. To our knowledge, the only other published work that has investigated the effects of this step-wise approach to aerosol forcing – that is prescribing a dry aerosol mass mixing ratio climatology versus fully interactive aerosols – was in the context of future climate (year 2100 emissions), rather than present day climate and did not include aerosol-climate coupling

of dust and sea salt aerosol [*Liao et al.*, 2009]. They found that including aerosol-climate coupling led to a positive feedback between decreased precipitation and increases in future aerosol concentrations and forcing. In a separate study, *Chung* [2006] found that prescribing aerosol forcing fields did not significantly affect global precipitation; however, many climate models, including the one used in this study, take the approach of prescribing aerosol mass, not aerosol forcing. Again, prescribing aerosol forcing (or wet optical properties) necessarily includes a prescription of aerosol hygroscopic growth and thus an assumption of relative humidity that may be inconsistent with the evolution of moisture fields in the host GCM.

[6] In Section 2 we describe the modeling system, the numerical experiments performed, and present an evaluation of the simulated aerosol optical properties and forcing relative to various observational datasets. Section 3 first describes the effect of simulated prognostic aerosols on the model climate, clouds, and zonal mean circulation (Section 3.1). We then compare and contrast these results to the effects of forcing the model with prescribed aerosol distributions for all aerosols and separately for natural (dust and sea salt) aerosols (Section 3.2). In Section 3.3 we examine the differences in aerosol optical depth between simulations with prognostic and prescribed aerosols, and we discuss reasons for these differences. Section 4 presents a discussion of the results followed by concluding remarks. Supplementary material provides additional detail on observational data and methods and additional figures and tables.

2. Experimental Design

2.1. GEOS-5 AGCM

[7] The GEOS-5 AGCM is one of the main components of the GEOS-5 atmospheric data assimilation system (DAS) and earth system model (ESM) [*Rienecker et al.*, 2008]. GEOS-5 is used to provide (1) research quality atmospheric reanalyses for use by the scientific community [e.g. the Modern-Era Retrospective Analysis for Research and Applications or MERRA, *Rienecker et al.*, 2011], (2) forward-processed analyses and forecasts for use by NASA instrument teams [e.g. *Zhu and Gelaro*, 2008], and (3) analyses and forecasts for use in various field campaigns [e.g. *Bian et al.*, 2012]. It has also been used as a tool to study aerosol impacts on weather [e.g. *Reale et al.*, 2011] and climate [e.g. *Ott et al.*, 2010]. Currently, efforts are underway to produce an aerosol reanalysis from assimilation of satellite-based aerosol optical depth (*da Silva et al.*, in preparation) GEOS-5 has the capability of operating as a free-running model (AGCM), a data assimilation system (DAS), or in a mode analogous to a CTM forced by reanalysis meteorology (replay).

[8] The GEOS-5 AGCM combines the finite volume dynamical core of *Lin* [2004] with a column physics package (turbulence based on *Lock et al.* [2000], relaxed Arakawa-Schubert (RAS) convection [*Moorthi and Suarez*, 1992], and a prognostic cloud scheme) and the catchment land-surface model of *Koster et al.* [2000]. Radiative transfer is computed using the parameterization of *Chou and Suarez* [1994, 2002] and *Chou et al.* [2003]. The model simulates traditional meteorological parameters (wind, temperature, pressure, etc.) [*Rienecker et al.*, 2008]. GEOS-5 also has modules representing atmospheric composition, including tropospheric aerosols [*Colarco et al.*, 2010] and

tropospheric and stratospheric chemistry [Pawson *et al.*, 2008], and incorporates the radiative impacts of these tracers online within the AGCM. The model domain can run at various horizontal spatial resolutions ranging from 2.0×2.5 latitude by longitude for climate studies to 0.25×0.3125 for data assimilation and atmospheric composition forecasts. There are 72 vertical layers distributed in a hybrid coordinate system that is terrain following near the surface transforming to pressure coordinates near 180 hPa (model top ~ 85 km). In this study, the AGCM was run at 2.0×2.5 latitude by longitude and forced by prescribed SSTs [Reynolds *et al.*, 2007].

[9] The prognostic aerosol module in GEOS-5 is based on the Goddard Chemistry, Aerosol, Radiation, and Transport (GOCART) model [Chin *et al.*, 2002]. It treats five tropospheric aerosol species (dust, sea salt, black carbon (BC), organic carbon (OC), and sulfate), including their sources, sinks, and chemistry. While dust, sea salt, and di-methyl sulfide emissions depend on the meteorological conditions in the underlying model (e.g. surface wind speed for dust and sea salt emissions), emissions for the other species are prescribed from emissions inventories (see Supplementary Material). Loss processes, including dry and wet deposition, for all species depend on model conditions (e.g. precipitation), as do the oxidation pathways for conversion of sulfur dioxide gas to sulfate aerosol (e.g. aqueous production).

[10] The aerosol species in GEOS-5 are treated as external mixtures that do not interact with each other, an assumption that has implications for aerosol optical properties because internal mixtures of absorbing and scattering aerosol components can greatly magnify aerosol absorption [e.g. Lesins *et al.*, 2002]. We are currently incorporating more detailed aerosol microphysics into GEOS-5 to permit internal mixing [e.g. including microphysical mechanisms as in Liu *et al.*, 2011]. With the exception of dust, optical properties are primarily from the commonly used OPAC data set [Hess *et al.*, 1998]; dust optical properties are derived from Aerosol Robotic Network (AERONET) measurements [Holben *et al.*, 1998] across the visible part of the spectrum and merged with OPAC in the longwave. Except for hydrophobic carbonaceous species and dust, aerosol optical properties are a function of the relative humidity in the underlying model (i.e. $AOD = \sum_{z,i} M_i \beta_{ext,i}$ where M_i and $\beta_{ext,i}$ are the mass [g m^{-2}] and mass extinction coefficient [$\text{m}^2 \text{g}^{-1}$] of species i , summed in the vertical (z) and over all aerosol species. β_{ext} is a non-linear function of RH for hygroscopic aerosols; see Supplementary Material Fig. S1 and Table S1). Further details of the GOCART aerosol module implementation and a validation with an earlier generation of the GEOS modeling system are given in Colarco *et al.* [2010].

[11] As noted earlier, the GOCART aerosol module has been integrated *online* in the AGCM. Thus, the aerosol transport, loss, and hygroscopic growth are consistent with the AGCM meteorological fields at every time step. Additionally, the aerosol tracers are radiatively coupled to the AGCM. The radiative forcing introduced by the aerosols thus provides the model both a direct radiative effect (DRE) and semi-direct effect (SDE) on the simulated climate. It is also possible to run the model where the transported GOCART aerosol fields are not radiatively coupled to the AGCM (i.e. as passive tracers). In this case, there is either no aerosol forcing, or else we impose the aerosol radiative forcing by prescribing

specified dry aerosol mass mixing ratio distributions (e.g. from a previous model run) to the radiative transfer module. The aerosol optical properties and forcing then depend on the prescribed dry aerosol mass and the model RH. The current version of the model does not include aerosol-cloud microphysical interactions, so in this study we do not consider a representation of the aerosol indirect effect.

2.2. Simulations

[12] We design a suite of numerical experiments for the GEOS-5 AGCM to test the importance of aerosol-meteorology coupling by including prognostic aerosols or prescribing consistent dry aerosol mass mixing ratio fields on a monthly-mean basis. In order to isolate the climate response due to aerosols from the internal model variability, we adopt 4-member ensembles starting from different initial meteorological conditions. Each ensemble member is run for the period 1999 to 2009, with the first year discarded as spin-up. Each ensemble mean (2000-2009) thus represents 40 years of simulation time. We run four different sets of ensembles, summarized in Table 1. In the first control ensemble, there is no aerosol forcing (NOAERO). In a second ensemble, the aerosols are dynamically and radiatively interactive and are derived from the prognostic GOCART scheme (GOAERO). In a third ensemble (CLIMAERO), the dry aerosol mass mixing ratio distributions are prescribed from the time-interpolated aerosol fields of the GOAERO ensemble mean (i.e. 11 years \times 12 months = 132 prescribed monthly mean dry aerosol mass distributions). This is so that on an inter-annual and monthly-mean basis the dry aerosol mass mixing ratios for the GOAERO ensemble mean and each of the four CLIMAERO ensemble members are the same. The GOAERO mass mixing ratios, however, vary at sub-monthly time intervals for each individual ensemble member. Importantly, while on a monthly-mean basis the GOAERO ensemble mean and CLIMAERO dry aerosol mass mixing ratios are identical, their aerosol optical properties (and forcing) are not necessarily the same even on a monthly-mean timescale because the non-linear dependence

Table 1. Simulations and signals.

Simulation	Aerosol Forcing ^a
NOAERO	None; control case
GOAERO	Interactive GOCART aerosols
CLIMAERO ^b	Prescribed dry aerosol mass mixing ratios from GOAERO
NATAERO ^b	Prescribed dust + sea salt dry aerosol mass mixing ratios from GOAERO
Signal ^c	Signal Source
INT	GOAERO – NOAERO
PRE	CLIMAERO – NOAERO
CPL	CLIMAERO – GOAERO or PRE – INT
NAT ^d	NATAERO – NOAERO

^aEach simulation consists of 4 ensemble members, each of which is run from 1999-2009, discarding 1999 as spin-up, for a total of 40-years of simulation for each ensemble mean.

^bMonthly-mean dry aerosol mass mixing ratios prescribed from GOAERO ensemble mean (11 years \times 12 months = 132).

^cINT = Interactive, PRE = Prescribed, CPL = Coupling, NAT = Natural

^dThe natural signal includes aerosol forcing from dust and sea salt only; for the purposes of this study biomass burning aerosol are not considered in this signal but are included in PRE. The dust and sea salt distributions in NATAERO are the same as those in CLIMAERO.

of aerosol optical properties on RH (see Supplementary Material), which may be different in each simulation. Our fourth ensemble (NATAERO) is constructed similarly to CLIMAERO but we prescribe only the dry aerosol mass mixing ratios for dust and sea salt aerosols.

[13] In discussing the aerosol direct and semi-direct effects on climate, we define signals as the difference between pairs of our ensembles (Table 1). The INT signal – the impact of interactive aerosols on climate – is the difference between the GOAERO ensemble mean and the NOAERO ensemble mean ($\text{INT} = \text{GOAERO} - \text{NOAERO}$). The PRE signal explores the impact of removing the coupling between model meteorology and aerosol distributions by prescribing aerosols ($\text{PRE} = \text{CLIMAERO} - \text{NOAERO}$). The NAT signal is the impact of prescribed natural dust and sea salt aerosols ($\text{NAT} = \text{NATAERO} - \text{NOAERO}$). By comparing the INT and PRE signals, we can examine the effect of having fully-coupled aerosols versus removing the effect of model meteorology on aerosol distributions. We define the coupling signal (CPL) as the effect of aerosol-climate interactions ($\text{CPL} = \text{PRE} - \text{INT} = \text{CLIMAERO} - \text{GOAERO}$).

[14] In all of our simulations, only the prescriptions of aerosol distributions differ; SSTs, long-lived GHGs, ozone, and oxidant fields are identical for all simulations. The ensemble simulations considered in this work cannot be considered to be without the influence of the real-world aerosols because we force the model with observed SSTs. On one hand, the strong control exerted by SST anomalies means that the simulations are able to capture major transport features [e.g. El Niño effects in the tropical atmosphere; *Ott et al.*, 2010]. On the other hand, SST changes due to simulated aerosol surface forcing are not realized. We thus neglect potentially important SST feedbacks on, for example, the hydrologic cycle. Because using prescribed SSTs represents an ocean with infinite heat capacity, the climate response to aerosol forcing may be representative of the response to forcing variations on intra-seasonal and shorter time scales when the ocean response would be delayed due to thermal inertia [*Lau et al.*, 2006; *Allen and Sherwood*, 2011]. We thus restrict our analysis to the aerosol forcing induced climate anomalies for the 10-year mean boreal (June-July-August or JJA) and austral (December-January-February or DJF) summers.

2.3. Evaluation of GOAERO aerosols

[15] As previously noted, the GEOS-5/GOCART aerosols have been extensively evaluated against ground- and space-based aerosol measurements. Results with a previous version of the system driven by reanalysis meteorology appear in *Colarco et al.* [2010]. Here we briefly examine the performance of the GEOS-5 aerosols driven by the simulated AGCM meteorology. We focus on the GOAERO simulation to establish the credibility and performance of the AGCM-derived aerosols compared to satellite observational data sets.

[16] We compare our simulated aerosol optical depth (AOD) to measurements provided by several satellite sensors. Sampling the model consistently with satellite orbital tracks as in *Colarco et al.* [2010; see Supplementary Material], the globally averaged ten-year AOD for GOAERO sampled with either the MODIS Terra or Aqua swath is 0.17 (compared to observed global mean AOD of 0.17 and 0.16 from MODIS

Terra and Aqua, respectively). Sampled with the MISR swath, the AOD for GOAERO is 0.18 (compared to 0.16 observed by MISR; see Fig. 1).

[17] Figure 1 (a-c) shows scatter plots of the monthly-mean, globally averaged aerosol optical depth (AOD) over land for the GOAERO ensemble mean relative to retrievals from MODIS Terra, MODIS Aqua, and MISR for the period 2000-2009 (i.e. 120 months). We see that there is generally good agreement (within ± 0.05 of the 1-1 line) between the model and observations over land during the boreal summer months, though in boreal winter months there tends to be a positive bias in the model AOD, particularly compared to MISR which provides retrievals of AOD over the Saharan dust region (Fig. 1 d-f). As shown in *Colarco et al.* [2010], the model simulated aerosols have similarities with the satellite observations, such as the position of the dust plume coming out of Africa, the Asian pollution plume crossing the northern Pacific Ocean, and the underestimate in AOD in biomass burning regions (e.g. South America, southern Africa) and over the Asian region (Fig. 1 d-f). We use substantially the same emissions inventories as in that study (see Supplementary Material). These types of features and biases are common in global aerosol models [e.g. *Textor et al.*, 2006].

[18] Compared to the results from GEOS-4/GOCART driven by reanalysis meteorology [*Colarco et al.*, 2010], the GOAERO simulation exacerbates the positive bias of AOD in dust and sea salt dominated regions (i.e. northern Africa and the Southern Ocean, respectively). The sea salt AOD bias is due to stronger winds in the Southern Ocean simulated by the climate model compared to the meteorological reanalysis (not shown). We also note that the satellite retrieval of AOD over the northern and southern hemisphere storm tracks likely suffers from cloud contamination [e.g. *Zhang and Reid*, 2006]. There is a high bias in the model AOD over Europe. *Colarco et al.* [2010] showed that this high bias and the high bias in the sea salt AOD over the Southern Ocean are somewhat reduced if the model is sampled where the satellite sensors *actually* make retrievals, rather than where they *could* make retrievals (as presented here). Our simulations are not tied to analysis meteorology and therefore do not correspond in time to actual sampling of the satellite observations, so we omit this screening in our comparisons.

[19] The top-of-the-atmosphere (TOA) all-sky (cloudy) instantaneous direct radiative forcing of anthropogenic and biomass burning aerosols (BC+OC+sulfate), globally averaged over the ten-year study period, is -0.41 W m^{-2} . The Intergovernmental Panel on Climate Change [IPCC; their figure TS.5 *Solomon et al.*, 2007] estimates the total aerosol direct radiative forcing for anthropogenic aerosols to be -0.5 W m^{-2} , with a range of -0.9 to -0.1 W m^{-2} , while biomass burning aerosols have a forcing of $-0.03 \pm 0.12 \text{ W m}^{-2}$. Our instantaneous forcing is calculated as the net (positive down) flux change at the top of the atmosphere with and without aerosols, holding atmospheric state fixed between two separate calls to the radiation module. Defined in this way, a positive TOA forcing indicates the addition of energy to the climate system (i.e. a radiative warming effect) whereas a negative effect indicates a net loss of energy (i.e. a radiative cooling effect). Note that for tropospheric aerosols that interact primarily with shortwave (SW) radiation, instantaneous forcing at the top-of-the-atmosphere

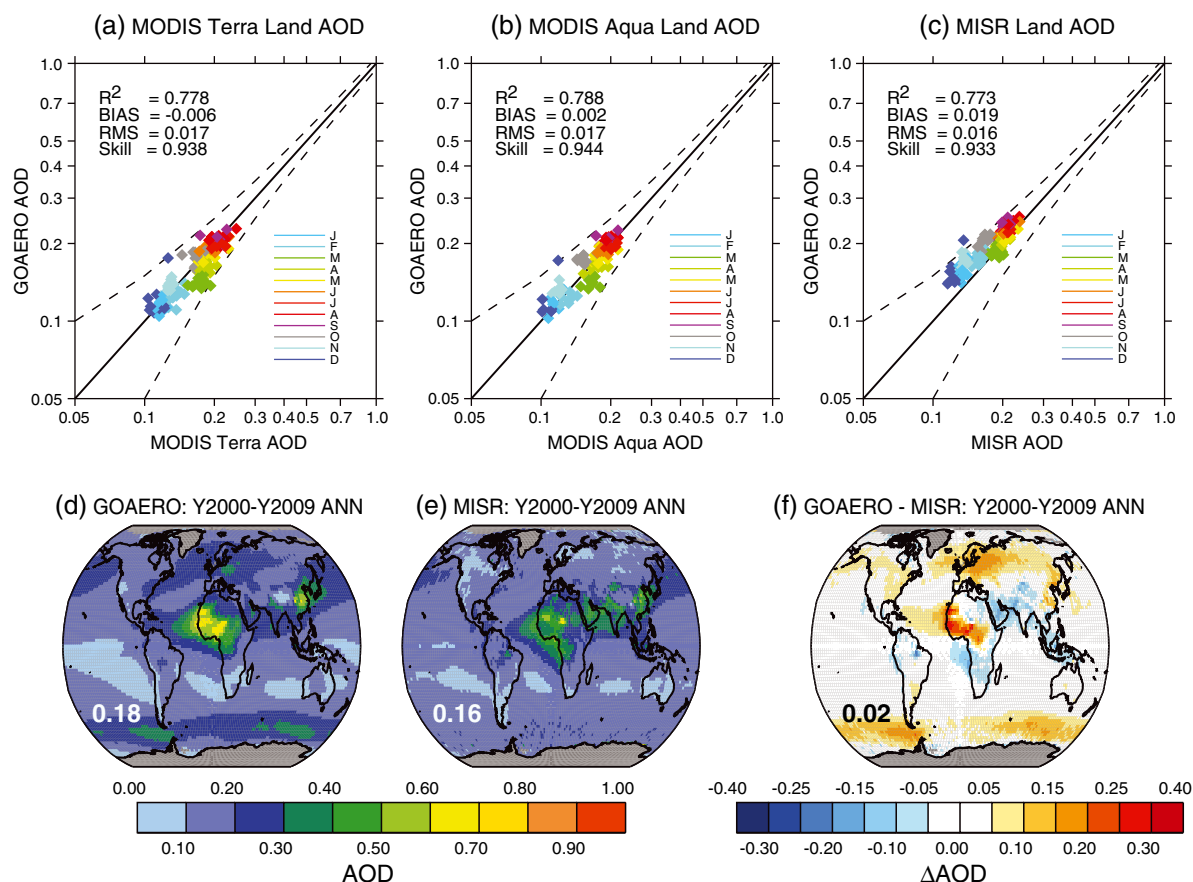


Figure 1. (a - c) Log-log comparison of monthly mean AOD globally averaged over land for the GOAERO ensemble mean compared to retrievals from the MODIS Terra, MODIS Aqua, and MISR sensors covering the period 2000 - 2009. Colors indicate the month, the solid black line is the 1-1 line, and the dashed lines are ± 0.05 from the 1-1 line. Statistics of the monthly mean comparison (R^2 , bias, rms, and skill score) are shown. (d - f) Annual average (2000-2009) AOD from (d) the GOAERO ensemble mean, (e) retrievals from MISR, and (f) the GOAERO ensemble mean bias relative to MISR (i.e. GOAERO - MISR). Global average values are given on each panel, and grey regions indicate regions where there is no data. The GOAERO ensemble mean has been sampled using the orbital swath of each sensor as described in the text and the Supplementary Material.

(TOA) and adjusted forcing as defined by the IPCC [Ramaswamy *et al.*, 2001] are approximately equal [Hansen *et al.*, 1997; Lohmann and Feichter, 2001]. In our GOAERO simulation, dust and sea-salt together have an instantaneous direct radiative effect (DRE) of -0.06 W m^{-2} . Here we distinguish the DRE, which refers to the atmospheric forcing from all aerosols (i.e. natural and anthropogenic), from the more

commonly examined direct aerosol radiative forcing (DARF), which only includes effects of anthropogenic aerosol [e.g. Yu *et al.*, 2006]. We find that the global, annual average DRE for our natural aerosol species generally lies within the range simulated by previous studies [e.g. Solomon *et al.*, 2007].

[20] It is also useful to examine the total aerosol forcing in the clear-sky case because this can be compared to

Table 2. GOAERO clear-sky instantaneous shortwave (SW) aerosol Direct Radiative Effect (DRE) over ocean (land) [W m^{-2}].^a

Simulation/Source	Clear-sky TOA DRE		Clear-Sky ATM DRE ^b		Clear-sky SFC DRE	
	Ocean (Land)	Ocean (Land)	Ocean (Land)	Ocean (Land)	Ocean (Land)	Ocean (Land)
GOAERO Clear-Sky Forcing	-4.8 (-4.5)		1.7 (3.8)		-6.5 (-8.3)	
Multi-Model Estimate [Yu <i>et al.</i> , 2006] ^c	-3.5 ± 0.64 (-2.8 ± 0.59)		1.3 (4.4)		-4.8 ± 0.80 (-7.2 ± 0.93)	
Observational Estimate [Yu <i>et al.</i> , 2006] ^c	-5.5 ± 0.21 (-4.9 ± 0.26)		3.3 (6.8)		-8.8 ± 0.67 (-11.7 ± 0.70)	

^aAnnual mean (2000-2009 average) for the GOAERO ensemble mean.

^bThe atmospheric direct radiative effect (DRE) is the difference between the top-of-the-atmosphere (TOA) and surface (SFC) DRE, i.e. ATM DRE = TOA DRE - SFC DRE.

^cMulti-model median and standard error estimated with different methods from GOCART, SPRINTARS, GISS, LMDZ-INCA, and LMDZ-LOA models. Multi-observational median and standard error estimated with different methods from MODIS, MISR, POLDER, SeaWIFS, and CERES data. (See Yu *et al.* [2006] Tables 7 and 8 and for further details). Note: ATM derived here as a difference between reported TOA and SFC estimates.

observationally based estimates. In Table 2 we give the clear-sky SW direct radiative effect (DRE) over land and ocean for the GOAERO ensemble mean, and we compare this to published estimates derived from multiple models and from satellite retrievals of aerosol optical properties and broadband flux measurements [Yu *et al.*, 2006]. There is about a 6% decrease in the magnitude of the TOA SW DRE over land versus over ocean due to the land/sea contrast in AOD, the contrast in surface albedo, and the presence of generally more absorbing aerosol over the land. The global, annual mean AOD for the GOAERO ensemble mean is 0.138 over ocean and 0.162 over land. Recall that TOA forcing is the sum of the atmospheric (ATM) and surface (SFC) forcing. The simulated clear-sky forcing in GOAERO is within about 10% of the observation-based DRE at the TOA; however there is less warming in the atmosphere (ATM) by about a factor of 2, leading to a larger difference in the SFC direct radiative effect. The GOAERO SFC forcing lies between the multi-model and observed estimates. The underestimate in aerosol absorption by a factor of 2 to 4 is common in global models [e.g. Sato *et al.*, 2003]. Part of the discrepancy between the modeled and observed DRE could be reduced by

accounting for cloud contamination in satellite retrievals [e.g. Yu *et al.*, 2006 and as discussed above].

3. Results

[21] Here we examine the direct and semi-direct aerosol impacts on climate in DJF and JJA. We show this first in Section 3.1 for the INT signal (GOAERO - NOAERO). In Section 3.2 we compare and contrast the impact of the online versus prescribed aerosol distributions, comparing the INT and PRE signals, and, equivalently, the CPL signal (i.e. $CPL = PRE - INT$). We also show the similarities between the CPL signal and the response to prescribed dust and sea salt aerosols (i.e. the NAT signal). In Section 3.3 we examine the sub-monthly variability of aerosol properties. Our purpose here is to flesh out differences between climate response to prognostic and interactive aerosols for a particular spatial distribution of aerosol (i.e. the CPL signal), and we caution that the response due to aerosols themselves (i.e. the INT, PRE, and NAT signals) is sensitive to the particular prescription of aerosols used, especially their vertical distribution [e.g. Ban-Weiss *et al.*, 2012 and Supplementary Material].

Table 3. Area-average impact of aerosols (direct and semi-direct effects) on seasonal climate (90% confidence).

Parameter ^c	INT (GOAERO - NOAERO) ^a				PRE/INT ^{a,b}			
	Land		Ocean		Land		Ocean	
	DJF	JJA	DJF	JJA	DJF	JJA	DJF	JJA
AOD	0.14	0.19	0.13	0.16	1.00	1.00	1.05	1.09
T2M	-0.21	-0.20	0.01	0.00	1.19	1.29	1.08	1.77
S850	0.06	0.09	0.00	-0.04	1.93	1.38	0.50	1.17
S500	0.19	0.23	0.05	0.05	1.35	1.08	1.00	0.68
PBLH	-9.83	-22.86	2.75	4.90	1.06	1.01	1.45	1.01
P	-0.05	-0.05	0.00	-0.02	1.02	1.08	1.33	0.76
EVAP	-0.03	-0.06	-0.01	-0.01	0.93	1.07	0.56	0.85
QA	-0.03	0.04	0.01	0.01	0.82	0.44	0.83	0.80
Q850	-0.03	0.03	0.02	0.03	0.28	0.82	1.00	0.81
TROPQ	0.66	1.48	0.70	0.76	0.83	0.98	0.96	0.98
RHBOT	0.15	0.45	0.05	0.01	1.16	1.05	0.89	1.30
OSR (↑)	1.33	2.16	2.96	2.93	1.07	1.04	1.04	1.03
OSRC (↑)	3.06	4.68	4.82	5.18	1.03	1.02	1.05	1.04
OLR (↑)	0.08	-0.68	-0.65	-0.83	1.32	0.97	0.82	0.82
OLRC (↑)	-0.94	-1.66	-1.35	-1.90	1.02	1.03	0.88	0.88
SWDWN (↓)	-5.22	-8.33	-4.72	-5.13	1.03	1.01	1.03	1.02
SWDWNC (↓)	-7.52	-11.32	-6.77	-7.55	1.02	1.01	1.04	1.03
LWDWN (↓)	0.56	1.45	1.51	1.83	0.88	0.77	1.00	1.00
LWDWNC (↓)	1.28	1.77	2.45	3.11	1.01	0.81	1.07	1.06
SFCEM (↑)	-1.33	-1.54	0.01	0.05	1.12	1.18	0.20	1.25
LWP	-0.41	-0.21	0.35	0.31	1.22	0.37	1.69	1.72
TAUTT	-0.34	-0.29	-0.11	0.04	1.00	1.00	1.13	0.80
CLDTT	-0.52	-0.29	0.07	-0.17	1.16	1.21	0.96	0.88
CLDLO	0.03	0.18	0.30	0.22	0.26	1.18	1.15	1.35
CLDMD	-0.10	0.03	0.00	0.02	1.49	0.59	2.00	1.24
CLDHI	-0.69	-0.57	-0.27	-0.49	1.08	1.10	1.03	1.07

^aStrikethrough text denotes changes that are NOT significant; otherwise, the INT and PRE signals are significant to the 90% confidence level determined by the t-test relative to the NOAERO control run as described in the text.

^bSignificance of CPL (i.e. CLIMAERO - GOAERO) determined relative to GOAERO; if the CPL signal IS significant to 90% confidence if the ratio above is in **bold italic** text; otherwise, CPL is NOT significant. Note: the CPL signal is for the difference CLIMAERO - GOAERO, not the ratio PRE/INT. It is possible for the PRE signal to NOT be significant (denoted by strikethrough text) even if the CPL signal IS significant (**bold italic** text).

^cAerosol Optical Depth (AOD) for GOAERO or CLIMAERO ensemble means. Change in (relative to NOAERO): 2-m air temperature (T2M; K); stability at 850 and 500 mb (S850 = $\Theta_{850} - \Theta_{2M}$; S500 = $\Theta_{500} - \Theta_{2M}$, where Θ is potential temperature; K); planetary boundary layer height (PBLH; m); total precipitation and evaporation (P and EVAP; mm d⁻¹); near-surface, 850 mb, and tropopause specific humidity (QA, Q850, and TROPQ; $\mu\text{g kg}^{-1}$ for surface and 850 mb, ng kg⁻¹ for tropopause); relative humidity in the bottom-most model layer (RHBOT, %); outgoing shortwave and longwave radiation at the top-of-the atmosphere in all and clear-sky (C) conditions (OSR, OSRC, OLR, and OLRC; positive upwards (↑), W m⁻²); downward shortwave and longwave radiation at the surface (SWDWN, LWDWN, SWDWNC, and LWDWNC; positive downwards (↓), W m⁻²); liquid water path (LWP; kg m⁻¹); cloud optical depth (TAUTT; unitless) total, low, mid, and high cloud amount (CLDTT, CLDLO, CLDMD, and CLDHI; %).

[22] Table 3 presents various climate-relevant parameters averaged separately over land and ocean in DJF and JJA (2000-2009 average) for the INT signal and the ratio of the prescribed signal to the interactive signal (PRE/INT). Results for the NAT signal are given in the Supplementary Material (Table S2). The INT, PRE, and NAT signals are statistically significant unless depicted with strikethrough text; we also indicate when the CPL signal (i.e. the difference CLIMAERO – GOAERO) is significant using bold-italicized text. The two-tailed Student's *t*-test statistic is used to determine the significance of each signal to 90% confidence [e.g. Wilks, 2006]. This statistic takes into account the means and standard deviations of both the control and perturbation ensembles; we examine seasonal anomalies for the 10-year mean period using the pooled variance. The control case is NOAERO for the INT, PRE, and NAT signals; for the CPL signal the control case is GOAERO. Additional information on the method for calculating statistical significance is given in the Supplementary Material. Note that the confidence level should not be interpreted as a measure of the accuracy of the model or its input, but it is a measure of the significance of the perturbation response relative to the model's natural internal variability [e.g. Erlick *et al.*, 2006].

3.1. Climate response to forcing from interactive aerosols

3.1.1. Temperature and Stability

[23] Figures 2a and 3a show the 2-m air temperature response to interactive aerosols in JJA and DJF, respectively, with stippling indicating changes that are significant to 90% confidence. The surface air temperature (T2M) response over land cools as expected due to decreased shortwave flux to the surface (SWDWN and SWDWNC, Table 3), and the cooler surface decreases the upward emission of longwave radiation (SFCEM). Prescribed SSTs limit the effect of aerosols on over-ocean surface air temperature, and a strong land/sea surface temperature contrast results. Other studies, including both those with fixed SSTs and those with coupling to slab ocean models, have also simulated a strong land-sea contrast in surface temperature response to aerosol radiative forcing [e.g. Allen and Sherwood, 2010]. Land in the northern hemisphere (NH) cools by a factor of 2-4 more than the southern hemisphere (SH) due to the peak of aerosol forcing in the NH (Fig. 1).

[24] Figures 2e and 3e show the zonal averaged temperature change for the INT signal. Throughout the midlatitudes and tropics, INT aerosols generally warm the troposphere significantly, with some near-surface cooling communicated to the atmosphere from the cooled surface (Fig. 2a and 3a). This atmospheric warming coupled with surface cooling tends to increase stability over land at 850 mb; at 500 mb the warming stabilizes the atmosphere over both land and ocean (S850 and S500; Table 3). In response to the increased stability, the planetary boundary layer height (PBLH; Table 3) decreases over land. The stratosphere warms for the INT signal. This warming is strongest in the polar region of the summer hemisphere. This radiative warming is primarily due to shortwave heating from aerosols (see Supplementary Material). However, particularly in the tropical stratosphere, some of this heating is likely a remote dynamical response to aerosol forcing [e.g. Allen and Sherwood, 2011, and Section 3.2 where we show that natural aerosols, which are confined to the troposphere, contribute to heating in this region].

3.1.2. Hydrologic Cycle

[25] Previous studies have shown that forcing from absorbing aerosols alone tends to enhance precipitation by warming the surface; however, this effect can be overwhelmed by the tendency of stronger shortwave heating of the atmosphere to suppress precipitation [Ming and Ramaswamy, 2011]. Studies that include both scattering and absorbing aerosols have shown that aerosols generally suppress precipitation [Chen *et al.*, 2011]. Globally, the INT signal, which includes forcing from both absorbing and scattering aerosols, indicates a decrease in precipitation (P; Table 3). We find that reduction in precipitation is stronger over land due to relatively higher aerosol loading and surface cooling. The area-average difference between precipitation (P) and evaporation (EVAP) indicates that there is a reduction of land moisture, particularly in DJF; averaged globally, however, P - EVAP is near zero.

[26] Figure 4 shows the JJA and DJF zonal-mean change in total column precipitable water (TPW; Fig. 4 a-b) and relative humidity in the lowest model layer (RHBOT; Fig. 4 c-d). The INT signal indicates a strong increase in both column-integrated water vapor and low-level relative humidity in the NH tropics and extratropics in JJA. The changes in both TPW and RH are strongest over northern Africa, the north Atlantic, the Arabian Sea, and parts of Asia (see Supplementary Material Fig. S4 and S5). In both DJF and JJA, the increase in atmospheric moisture and air temperature serve to increase the downward flux of longwave radiation to the surface in all- and clear-sky conditions (LWDWN and LWDWNC; Table 3). The specific humidity near the surface and at 850 mb (QA and Q850; Table 3) increase over the ocean where increased stability inhibits vertical motion and traps moisture [Allen and Sherwood, 2010].

3.1.3. Clouds

[27] We now consider the effect of interactive aerosols on clouds. Recall that we do not consider aerosol indirect effects in this study; therefore, aerosol impacts on clouds are due either to the thermodynamic effect (semi-direct effect) or to dynamical responses to aerosol forcing. Table 3 shows the area-average land and sea changes in low- (CLDLO; cloud-top pressure > 680 mb), mid- (CLDMD; 680 mb > cloud-top pressure > 440 mb), and high- (CLDHI; 440 > cloud-top pressure) level cloud amount. The INT signal exhibits an increase in low-level clouds, particularly over the ocean. The global, annual mean increase in low-level clouds (0.21% and 0.22% in JJA and DJF, respectively) is close to the range (0.14-0.21%) reported in Wang [2004] and is similar to the findings of Bauer and Menon [2012]. We also simulate a land-sea contrast in low-cloud changes similar to the results of Allen and Sherwood [2010] who postulated that the increase in oceanic low-cloud was due to the increased stability and moisture trapping near the surface induced by aerosol heating of the atmosphere. Low-cloud amount increases are particularly strong in regions dominated by marine stratocumulus (e.g. off the western coasts of North and South America and southern Africa; Fig 5a and 6a), areas where low-clouds are expected to increase with increased stability [e.g. Klein and Hartmann, 1993]. However, this increase in low-level cloud is a counter example to the common understanding of the semi-direct effect [e.g. Perlwitz and Miller, 2010].

[28] Our simulations show little change in mid-level clouds and large decreases in high-level clouds, especially

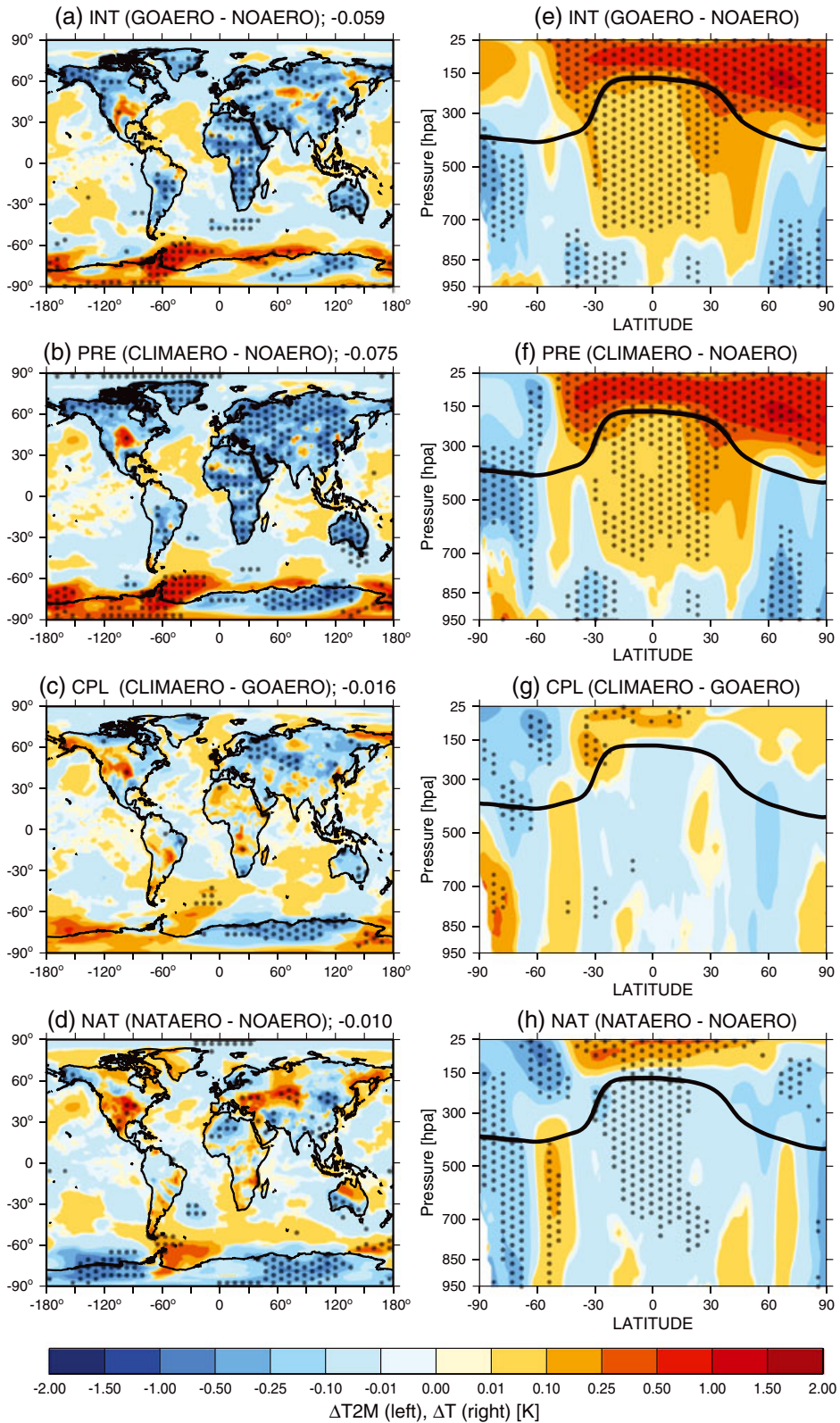


Figure 2. JJA (2000 - 2009) change in (a - d) 2-m air temperature (T2M; K) and (e - h) zonally averaged air temperature (T; K) for the signals in Table 1. The global average is indicated on each panel for the 2-m air temperature change, and significant (90% confidence) changes, as determined by the t-test, are indicated by stippling. The tropopause level is plotted in (e - h) for the respective control case (NOAERO or GOAERO).

over land (Table 3). This contrasts with the findings of *Allen and Sherwood* [2010] who found large decreases in mid-

level clouds and increases high-level clouds, particularly over land. However in their study aerosol forcing was only

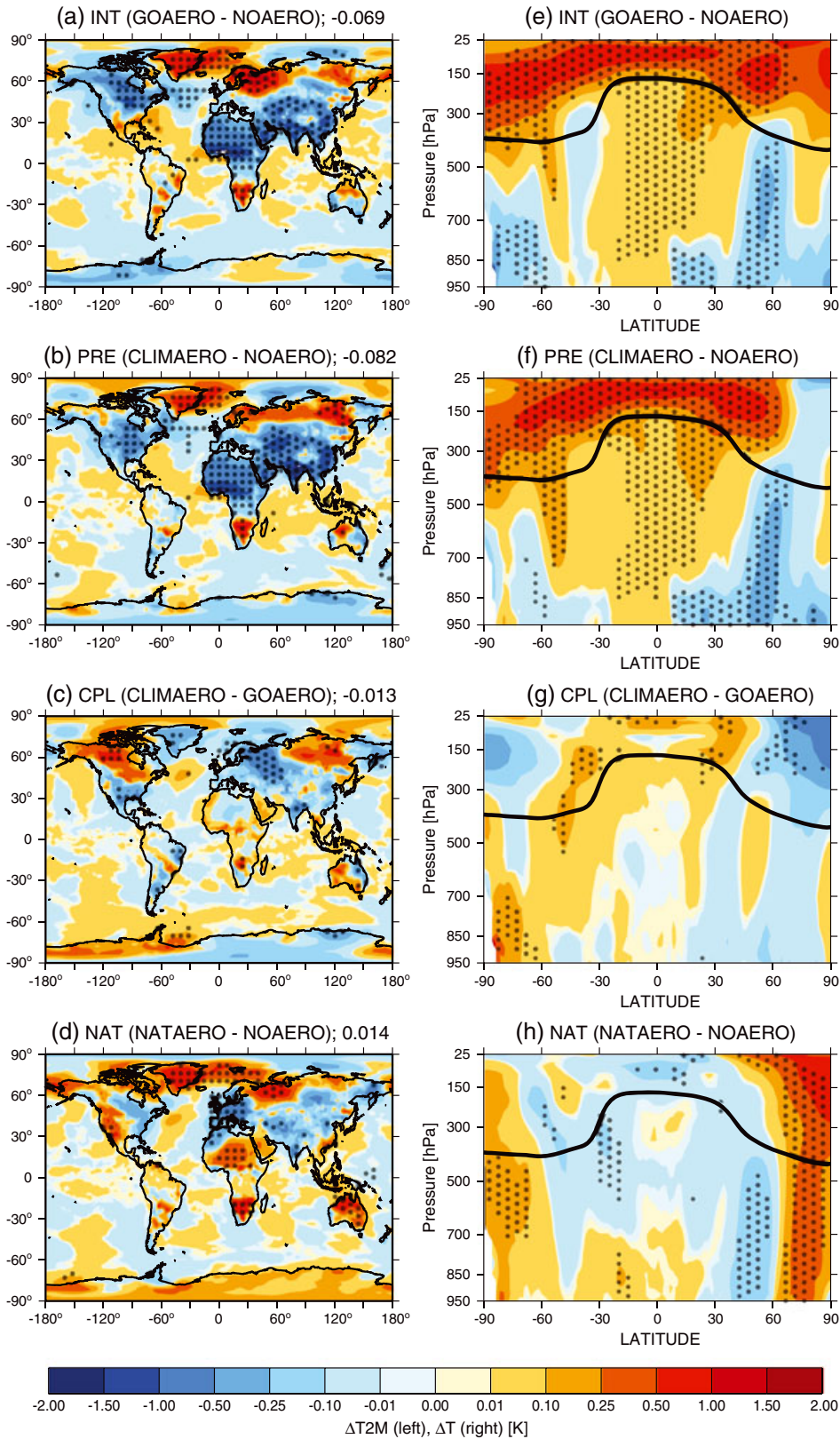


Figure 3. Same as Figure 2 but for DJF.

applied to the lowest 3 km of the model, and only anthropogenic aerosol forcing was considered. The global decrease in high-level clouds is consistent with the response to dust forcing considered by *Perlwitz and Miller* [2010] and with the

response to black carbon aerosol above 4 km considered in *Ban-Weiss et al.* [2012]. Outgoing longwave radiation (OLR) increases where high and mid-level clouds decrease (not shown); however, the overall negative change in OLR

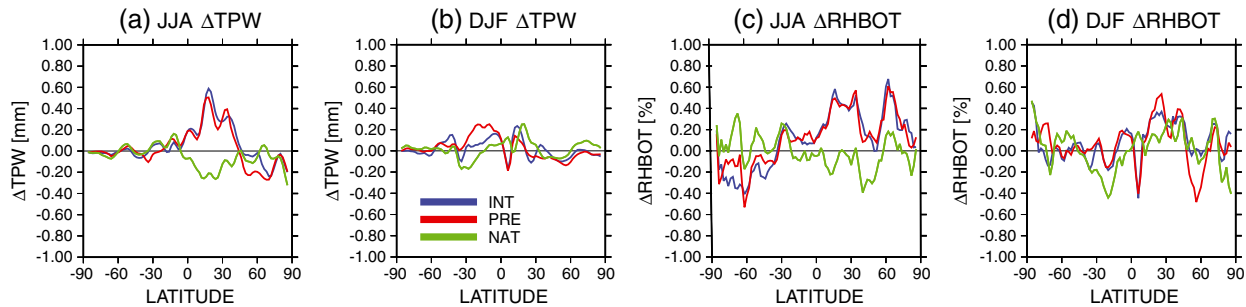


Figure 4. Change in (a - b) zonally averaged total column precipitable water vapor (TPW; mm) and (c - d) zonally averaged relative humidity in the bottom model layer (RHBOT, %) for the INT, PRE, and NAT signals (Table 1). Recall the CPL signal is equivalent to the PRE – INT signal. See Supplementary Figs. S4 and S5 for the spatial distributions of TPW and RHBOT in JJA and DJF, respectively.

is dominated by the increase in atmospheric water vapor (e.g. clear-sky decrease OLRC in Table 3) and is therefore stronger in JJA (see TPW in Fig. 4).

[29] Globally-averaged total cloud amount decreases by -0.21 and -0.11% in JJA and DJF, respectively (see Supplementary Fig. S6 and S7). This overall decrease in total clouds (CLDTT) implies a globally positive (warming) semi-direct effect. Indeed, we find that the inclusion of aerosols decreases shortwave cloud radiative cooling while also decreasing longwave cloud radiative warming such that the net effect of cloud changes is a radiative warming. We caution, however, that changes in cloud radiative forcing are due both to the semi-direct effect and to any changes in global circulation that may occur in response to aerosol radiative forcing. Further, the SDE is highly sensitive to the vertical distribution of absorbing aerosols [e.g. *Ban-Weiss et al.*, 2012 and Supplementary Material].

[30] Cloud optical thickness decreases over land, and to a lesser extent over ocean (TAUTT; Table 3). As pointed out by *Bauer and Menon* [2012], decreases in cloud optical thickness due to direct and semi-direct aerosol effects may counterbalance cloud optical depth increases associated with increased CCN (i.e. aerosol indirect effects assuming constant cloud liquid water path), which we do not consider in this study. Cloud liquid water path (LWP; Table 3) decreases over the land, except in the Sahel region of northern Africa in JJA (not shown). *Sakaeda et al.* [2011] also simulated decreased cloud liquid water path over the Sahel, where reduced LWP dominated the reductions in cloud amount in determining their positive semi-direct effect in this region. The increased LWP and low cloud amount over the ocean are consistent with the effects of aerosol absorption above cloud decks that reduces cloud-top entrainment and increases cloud thickness [*Wilcox*, 2010, 2012; *Johnson et al.*, 2004].

[31] Figures 5e and 6e show the zonally averaged change in RH (shading) and cloud fraction (FCLD; contours) (see Supplementary Figs. S6 and S7 for FCLD shaded). The INT signal shows increases in low-level clouds, increases in cloud fraction throughout the tropospheric column in the high latitudes, and decreased high clouds near the tropopause in the summer hemisphere. Both the increases and decreases in cloud amount mirror the changes in relative humidity. For example, there is a large decrease in relative humidity associated with the atmospheric warming near the tropopause in the summer hemisphere (Fig. 2e and 3e) that

explains the decrease of high-level clouds near the tropopause. Increased RH near the surface accompanies increases in the low-level cloud amount (e.g. near 30S in JJA). We expect these correlations in low cloud amount and RH because GEOS-5 diagnoses stratiform clouds based on a PDF of total water [*Smith*, 1990; *Rotstayn*, 1997; *Rienecker et al.*, 2008].

3.1.4. Circulation

[32] Figures 7 and 8 show the changes in the mean meridional mass circulation or mass stream function (MMC, a-d) and the zonal mean wind (U, e-h) for the signals in Table 1 in JJA and DJF, respectively. In JJA (Fig. 7a), forcing by all aerosols weakens the ascending branch of the Hadley cell near 15°N (less negative MMC), but subsidence is enhanced in the SH north of 30°S in the lower troposphere (more negative MMC). These changes concur with the increases in low-level stability (Table 3). The increased subsidence helps to trap moisture near the surface and contributes to increased low-level cloud and moisture, particularly over the oceans (see Figs. 4-6). In the Southern Ocean near 60°S, the INT signal indicates increased upward motion, which likely contributes to increases in clouds and RH throughout the column in this region (Fig. 5e). In DJF, the descending branch of the Hadley cell (~20°N) is significantly enhanced in the lower troposphere by the INT aerosols (Fig. 8a); FCLD and RH are increased near the surface in the INT case in this same region (Fig. 6e).

[33] Figures 7 and 8 indicate a strengthening of the zonal mean wind near 60°N and 60°S in JJA and near 45°N and 30°S in DJF. As in *Allen and Sherwood* [2011], we determine the location of the midlatitude jets by first interpolating the zonal wind to 0.5 resolution and then locating the maximum wind in each hemisphere for each year and month in the upper troposphere (250-150 hPa). To determine the meridional displacement of the jet, we then averaged over seasons and determine the climate signals (i.e. experiment - control) in Table 1. The NH jet displaces poleward by 0.43 and 0.20 degrees in JJA and DJF, respectively (see Figs. 7e and 8e); however the SH displacement is much smaller not significant to 90% confidence. This is expected since other studies have shown that stratospheric ozone depletion is the main driver of the SH jet shift [*Kang et al.*, 2011]. *Allen and Sherwood* [2011] found a significant poleward displacement of the NH jet in response to anthropogenic aerosol forcing (up to 0.42 in SON), and that poleward shift in the location of the subtropical jets in JJA implies an expansion of the tropics. GCM-studies of global warming have linked

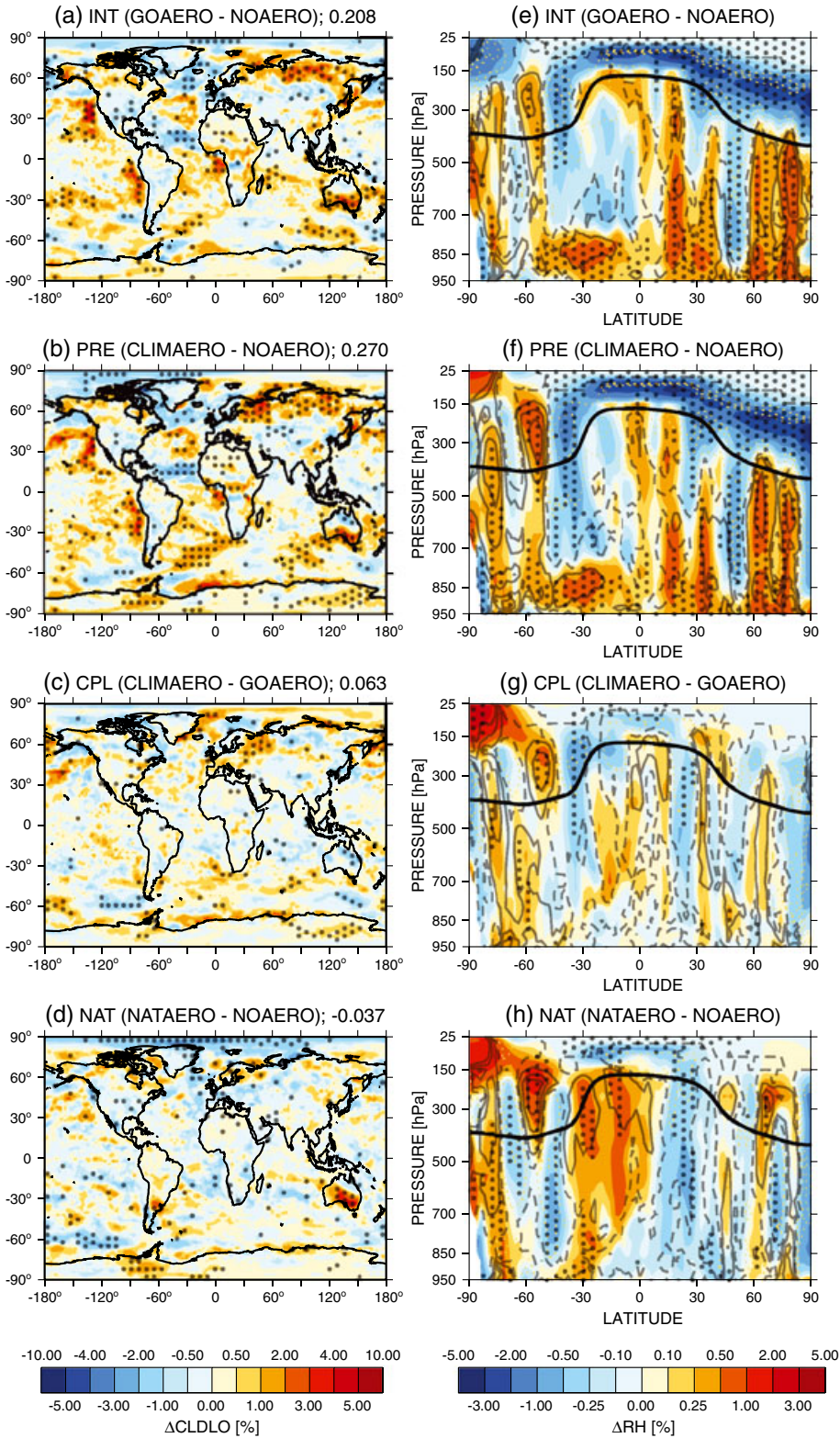


Figure 5. JJA (2000 - 2009 average) change in (a - d) low-level cloud amount (CLDLO; %; shaded) for the signals in Table 1. (e - h) Change in zonally averaged relative humidity (RH; %, shaded) and change in zonally averaged cloud fraction (FCLD; %; solid (dashed) contours are increased (decreased) RH with contours of ± 0.1 , ± 0.3 , and ± 0.5). The global average is indicated on each panel for the low-level cloud amount, and significant (90% confidence) changes in CLDLO and RH, as determined by the t-test, are indicated by stippling. The tropopause level is plotted in (e - h) for the respective control case (NOAERO or GOAERO). See Supplementary Fig. S6 for total cloud changes (CLDTT, %) and zonally averaged cloud fraction (FCLD, %) in shading.

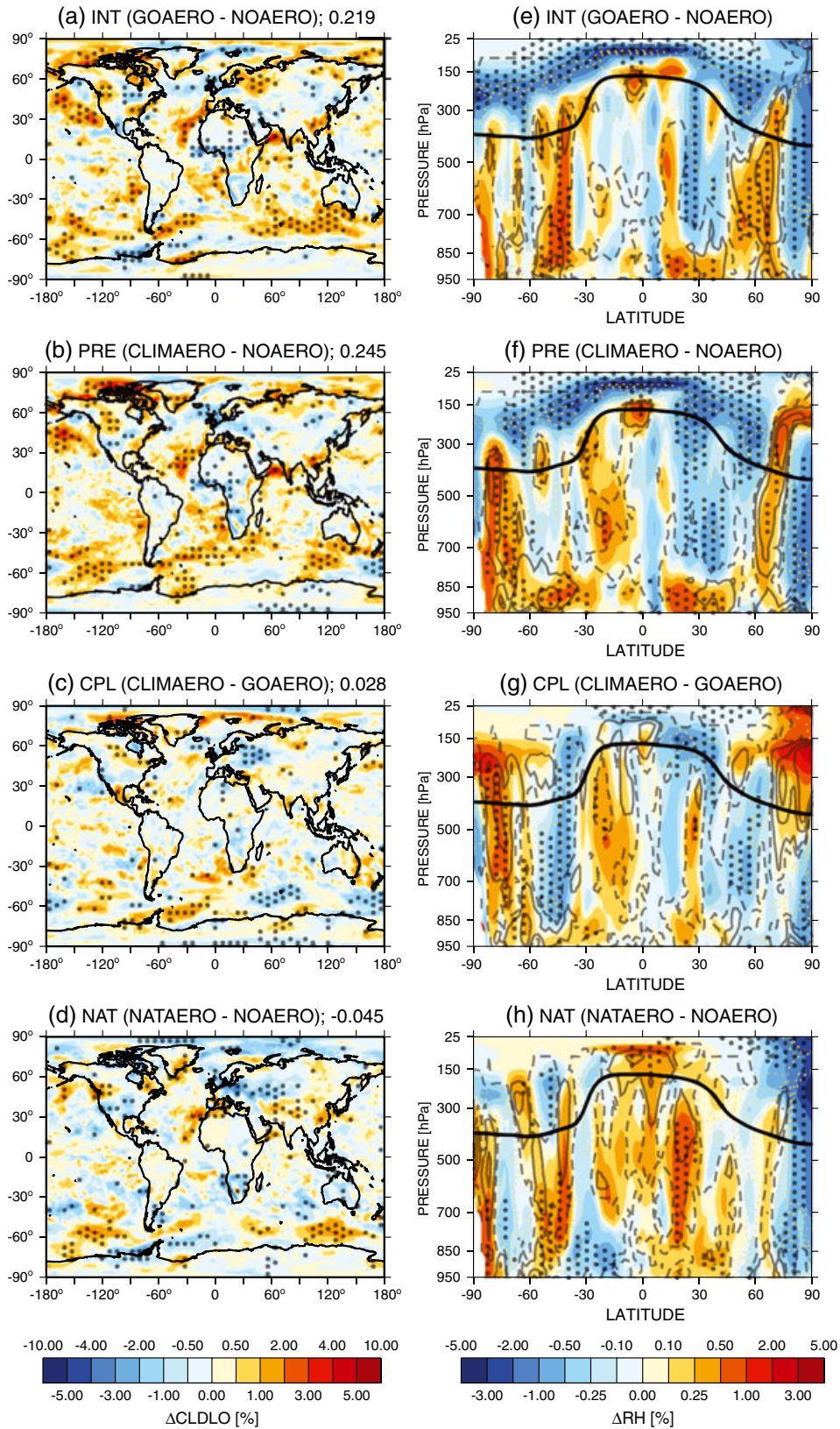


Figure 6. Same as Figure 5 but for DJF. See Supplementary Fig. S7 for total cloud changes (CLDTT, %) and zonally averaged cloud fraction (FCLD, %) in shading.

the poleward displacement of the subtropical jet and storm tracks and the expansion of the Hadley circulation to increased subtropical stability [e.g. Frierson *et al.*, 2007;

Lu et al., 2008]. Recent evidence suggests that tropospheric heating due to black carbon aerosol is a likely driver of the NH tropical expansion seen in the observational record

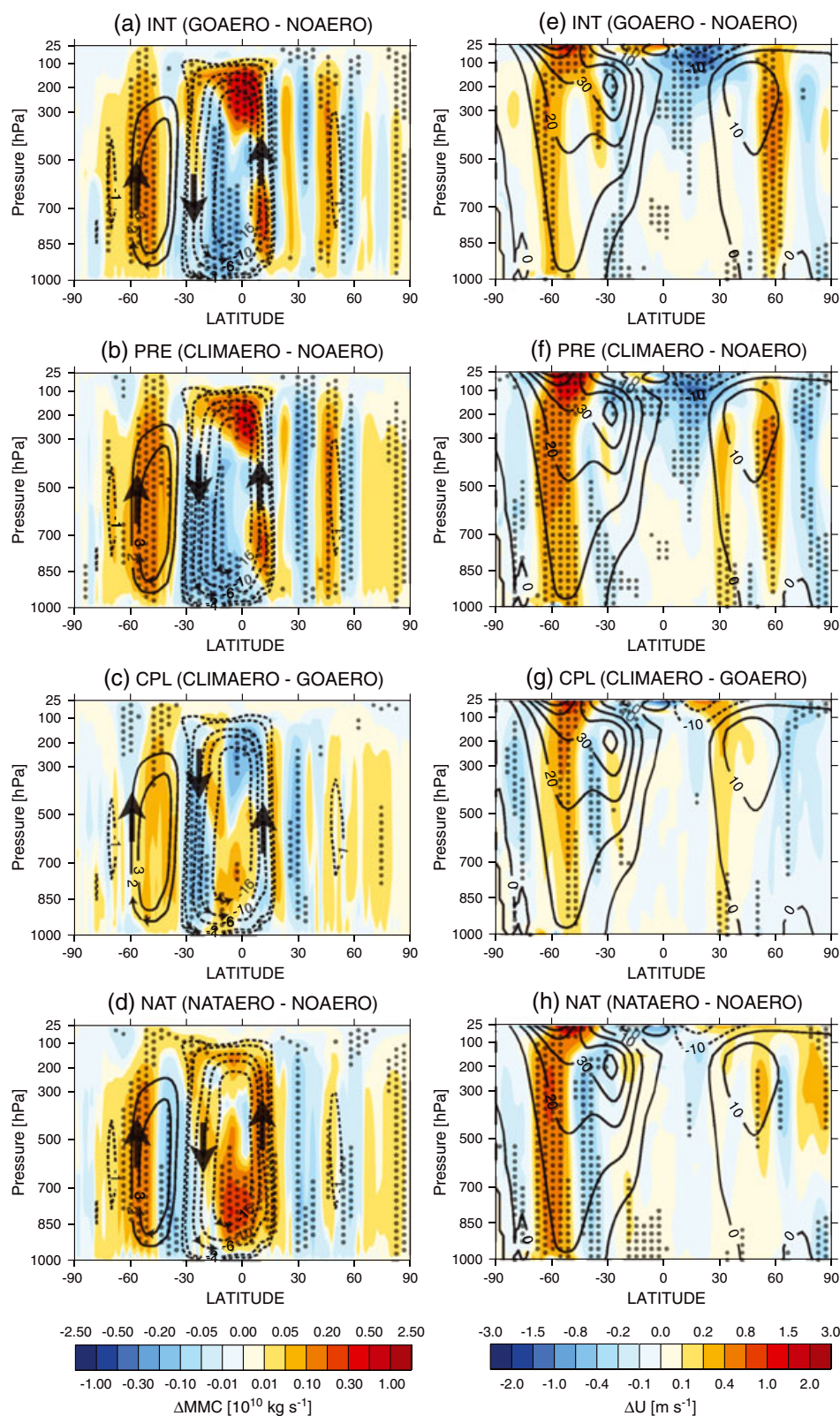


Figure 7. JJA (2000 - 2009 average) change in (a - d) mean meridional circulation or mass stream function (MMC; $10^{10} \text{ kg s}^{-1}$; shaded) and (e - f) zonal wind speed (U ; m s^{-1} ; shaded) for the signals in Table 1. Significant (90% confidence) changes, as determined by the t-test, are indicated by stippling. The MMC and zonal mean wind for the respective control case (NOAERO or GOAERO) are plotted with black contours with positive (negative) values plotted with solid (dashed) contours. For the MMC, the sense of the circulation is indicated by arrows with the control case contours. See Supplementary Fig. S8 for changes in zonal mean wind in the bottom-most model layer.

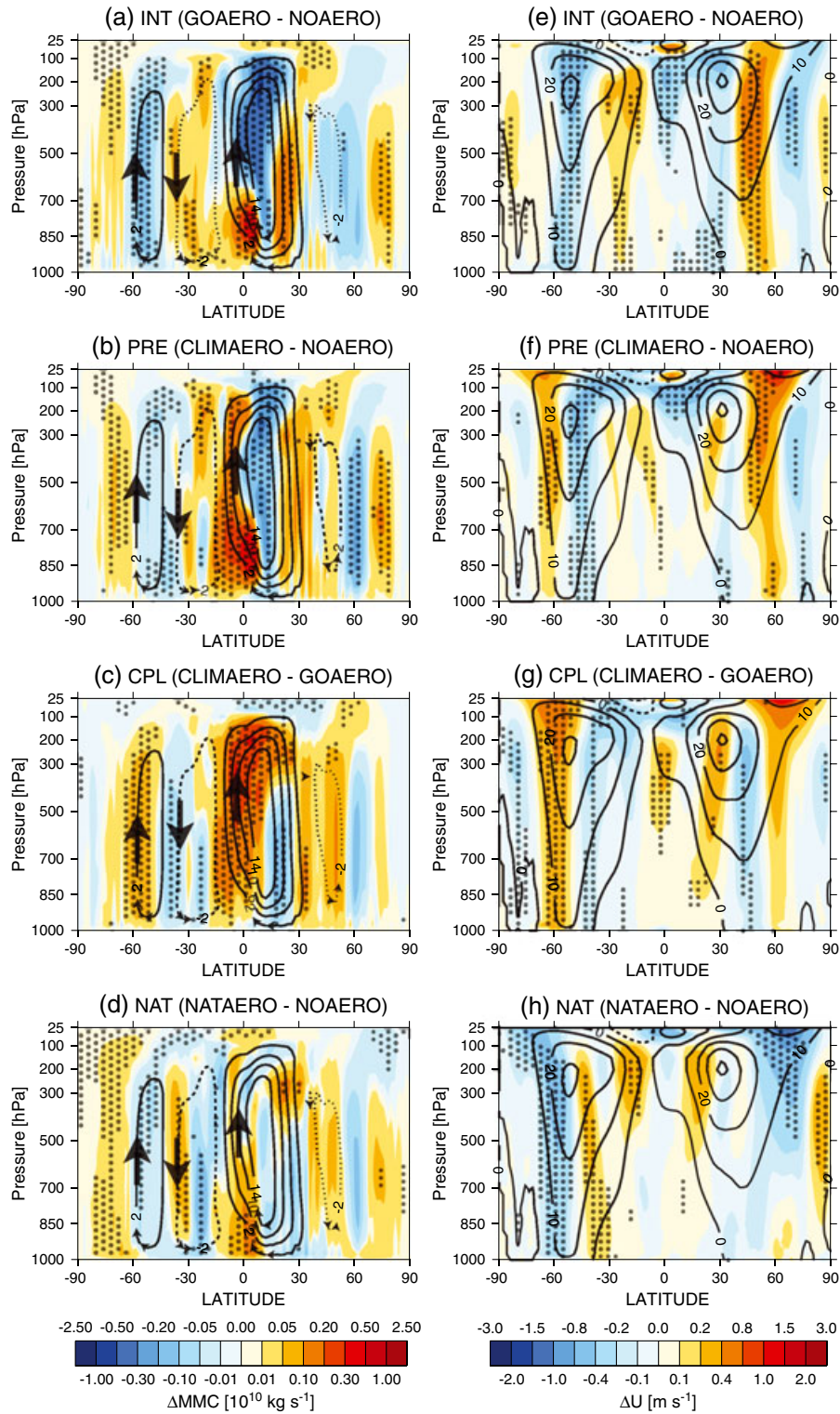


Figure 8. Same as Figure 7 but for DJF.

[Allen et al., 2012a, b]. Aerosols also affect mid- and high-latitude winds near the surface, a measure of the storm tracks (see Supplementary Fig. S8). As in Allen and Sherwood [2011], the INT signal shows slight poleward shifts in low-level winds in the winter hemisphere, consistent with a poleward shift in the storm tracks.

3.2. Effects of prescribed aerosols and aerosol-meteorology coupling

[34] We now examine the impacts of aerosol-meteorology coupling by comparing and contrasting the PRE and INT signals. Recall that we have defined the coupling signal (CPL) as the difference between the PRE and INT signals,

or, alternatively as the difference CLIMAERO - GOAERO (Table 1). We assess the statistical significance of both the PRE signal (i.e. the significance of the CLIMAERO - NOAERO anomaly), as well as the significance of the CLIMAERO - GOAERO anomaly (the CPL signal) relative to their respective control cases (NOAERO or GOAERO).

[35] In Table 3, we show the ratio of the PRE to INT signals for area averaged climate parameters. We see that the sign of the PRE and INT signals are generally the same for all climate parameters considered; similarly, climate signals that are significant for the INT signal are also significant for the PRE signal (i.e. the climate change due to aerosols relative to no aerosols is similar in sign and significance for both interactive and prescribed aerosols). The significance of the CPL signal (CLIMAERO - GOAERO denoted by bold italic text in Table 3), however, indicates that the magnitude of the PRE and INT signals differs significantly for numerous area-average climate parameters.

[36] Land-area average surface air temperature cools about 20-30% more for prescribed aerosols relative to interactive aerosols. Area-averaged stability at 850 mb over land is increased by roughly a factor of two for prescribed aerosols in DJF and 40% in JJA (Table 3). However, despite these differences in area-averaged surface cooling, the spatial distribution of surface temperatures is remarkably similar in the tropics (Fig. 2 and 3 a-b). Indeed, the CPL T2M signal indicates the majority of statistically significant changes lie poleward of roughly 30° (Fig. 2c and 3c). Interestingly, the high-latitude surface air temperature CPL signal has a wave-like structure, particularly in the winter hemisphere. *Allen and Sherwood* [2011] found an Arctic Oscillation (AO)-type high latitude response to anthropogenic aerosol forcing in winter under conditions of fixed SSTs. Our 2-m air temperature change for both the PRE and INT signals also exhibit a strong high-latitude response in the winter hemisphere. The CPL signal indicates, however, that the spatial structure of this response differs depending on the use of interactive or prescribed aerosols. The largest differences in zonally averaged tropospheric temperature change between the INT and PRE signals are also found in the extratropics (Fig. 2g and 3g). However, most of the CPL signal in the troposphere is not statistically significant. The CPL stratospheric temperature signal is significant in the tropics and the high latitudes of the winter hemisphere, remote from most direct aerosol forcing. This indicates that these differences may be dynamical in nature.

[37] As in *Chung* [2006], we do not find large differences in area-averaged precipitation and evaporation between simulations forced with interactive and prescribed aerosols. This indicates that the prescribed SSTs exert more control over the precipitation changes than does the aerosol-meteorology coupling considered here. However, we do see a significant change in the amount of water vapor in the atmosphere (Table 3). Specific humidity changes are significantly larger in magnitude over land for prescribed aerosols compared to interactive aerosols (QA, Q850, TROPQ). Globally, total precipitable water (TPW) increases less for the PRE signal compared to the INT signal in JJA (Fig. 4 and Supplementary Figs. S4 and S5). This relative decrease in atmospheric water vapor content when aerosols are prescribed results in less of a reduction of downwards long-wave radiation at the surface compared to the INT signal

(LWDWN, LWDWNC; Table 3). However, despite having atmospheric water vapor changes that are lower in magnitude compared to interactive aerosols, the CPL signal indicates that PRE aerosols tend to increase relative humidity, which depends both on atmospheric water vapor content and temperature (RHBOT; Table 3, Fig. 4, and Supplementary Figs. S4 and S5).

[38] The CPL signal indicates that prescribed aerosols tend to strengthen the descending branch (increased subsidence) of the Hadley circulation in the SH tropics ($\sim 30^\circ\text{S}$) in JJA more than interactive aerosols (Fig. 7c), in accord with the strengthening of lower-tropospheric stability (Table 3) and the increase in low-level clouds in this region (Fig. 5g). In DJF, there is more tropical ascent in the PRE signal compared to the INT signal (Fig. 8c), but weaker descent near 30°N , where we find a relative decrease in RH and cloud amount (Fig. 6g).

[39] The differences in zonal mean wind between the PRE and INT signals are related to differences in temperature gradient. In JJA, the CPL signal (Fig. 2g) indicates a significant difference in the INT versus PRE north-south temperature gradient in the SH, particularly in the stratosphere. The thermal wind equation dictates stronger westerlies for a stronger temperature gradient, as seen in Figure 7g. In the NH, where there is less of difference in temperature gradient, the zonal wind changes are weaker and less significant for the CPL signal. We find that the NH jet is only displaced northward by 0.17° when we force with prescribed aerosols, which is roughly half as much as when we force by interactive aerosols and not statistically significant. In DJF, again the stronger north-south temperature gradient in the PRE signal (Fig. 3g), this time in both hemispheres, tends to strengthen the zonal wind more when aerosols are prescribed (Fig. 8g). The NH jet shifts northwards by 0.12° , but this shift is not statistically significant.

[40] We also examine the impact of prescribing only the natural (dust and sea salt aerosols) from the same aerosol dry mass climatology as the CLIMAERO ensemble. Previous studies of the direct and semi-direct effects of aerosols have found opposing climate impacts for scattering and absorbing aerosols [e.g. *Randles and Ramaswamy*, 2008, 2010] or for natural and anthropogenic aerosols [e.g. *Allen and Sherwood*, 2011], the latter of which tend to have stronger atmospheric forcing globally. Recall from Section 2.3 that the instantaneous TOA forcing of dust and sea salt aerosols in our simulations was close to zero (-0.06 W m^{-2}). We have only a slightly positive atmospheric forcing due to natural aerosols (0.01 W m^{-2}), roughly 2% of the anthropogenic and biomass burning atmospheric forcing. Owing to the differences in radiative forcing, we expect the climate response to these natural aerosols alone to be much weaker than for either the INT or PRE signals. Indeed, many globally averaged parameters are not significant relative to the NOAERO control simulation (see Supplementary Table S2). However, it is important to note that global averages may mask regional signals that can be significant.

[41] We compare the NAT and PRE signals, which share the same prescribed sea salt and dust dry aerosol mass distributions. Because the NAT and PRE signals are both influenced by the same dust and sea salt aerosols, we expect the PRE signal to be a convolution of the response to natural and anthropogenic aerosols. Globally, the effect of natural

aerosols on land surface air temperature is small (Fig. 2-3). In JJA, natural aerosols warm the tropical stratosphere, which agrees with the findings of *Allen and Sherwood* [2011] who postulated this to be a remote dynamical response to aerosol forcing, though the cause of this remains unclear. The tropical stratospheric cooling in DJF due to natural aerosols is also consistent with fixed SST results from *Allen and Sherwood* [2011].

[42] An interesting observation is the similarity between the CPL signal (Fig. 2g) and the NAT signal (Fig. 2h) for the zonal mean temperature change in JJA, particularly the tropical stratospheric warming and tropospheric warming near 60°S. If we assume that the temperature response in the southern hemisphere troposphere and the tropical stratosphere is heavily influenced by natural aerosols in boreal summer, then the similarity between the CPL and NAT signals in JJA indicates that the differences between the PRE and INT signals is primarily due to differences in their dust and sea salt forcing. As we show in Section 3.3, we might expect this since sea salt dominates the AOD in the SH and we have higher oceanic AOD, particularly over the Southern Ocean, in the PRE case compared to the INT case (see Fig. 9). We do not, however, find such strong similarities between the CPL and NAT signals in DJF.

[43] The CPL and NAT similarities and SH temperature response extend to the zonal mean circulation changes in JJA. Both total aerosol forcing (PRE) and forcing from natural aerosols alone (NAT) act to increase zonal mean wind near 60°S (Fig. 7). Increases in the zonal mean wind in this region are weaker in the INT case (thus a positive CPL signal in this region). In DJF, however, as in *Allen and Sherwood* [2011], natural aerosols tend to increase the zonal wind equatorward of the jet maximum, and the opposite response results when total aerosol forcing is considered (PRE). The JJA NH jet displacement is insignificant for the NAT signal; however, in DJF the SH jet is displaced equatorward by 0.4 degrees. *Allen and Sherwood* [2011] show that the equatorward displacement of the subtropical jet by natural aerosols is consistent with a contraction of

the tropics. In JJA, natural aerosols generally weaken the Hadley cell (Fig. 7) as in *Allen and Sherwood* [2011], and in DJF they somewhat strengthen it near the equator (Fig. 8).

3.3. The effect of aerosol-meteorology coupling on AOD

[44] Figure 9 (a-b) shows the difference in AOD between the GOAERO and CLIMAERO ensemble means (i.e. the CPL signal) in JJA and DJF. Globally and annually averaged, AOD is 3% higher in CLIMAERO compared to GOAERO. Similar increases are found in JJA and DJF (Table 3). Most of the significant increases are found over the oceans, particularly at higher latitudes where the storm tracks reside. Over the land, especially near strong anthropogenic aerosol source regions such as in Asia, AOD is higher in GOAERO. These differences in AOD have consequences for the total aerosol forcing. Prescribed aerosols (CLIMAERO) exert a TOA clear-sky cooling 6% greater than interactive aerosols (GOAERO) over the ocean and 2% greater over land. Clear- and all-sky SW downwelling flux reduction is greater over both land and ocean when aerosols are prescribed (Table 3). Clear-sky outgoing shortwave radiation significantly increases for the PRE signal (CLIMAERO - NOAERO) relative to the INT signal (GOAERO - NOAERO), in summer and over the ocean. These differences in forcing ultimately impact the climate response of the model.

[45] The CLIMAERO and GOAERO ensemble means have the same monthly mean aerosol mass loading and vertical distribution, so the question naturally arises as to what factors are driving their differences in AOD. We consider two possibilities: (1) variability in the GOAERO aerosol loading on sub-monthly timescales and (2) variability in the RH environment between GOAERO and CLIMAERO. Recall that all ensemble members of CLIMAERO have fixed aerosol mass concentration and vertical distribution across a month equivalent to the ensemble mean from GOAERO. However, both individual ensemble members from GOAERO and the GOAERO ensemble mean may have considerable variability in mass loading at sub-monthly timescales. Despite such differences in the sub-monthly

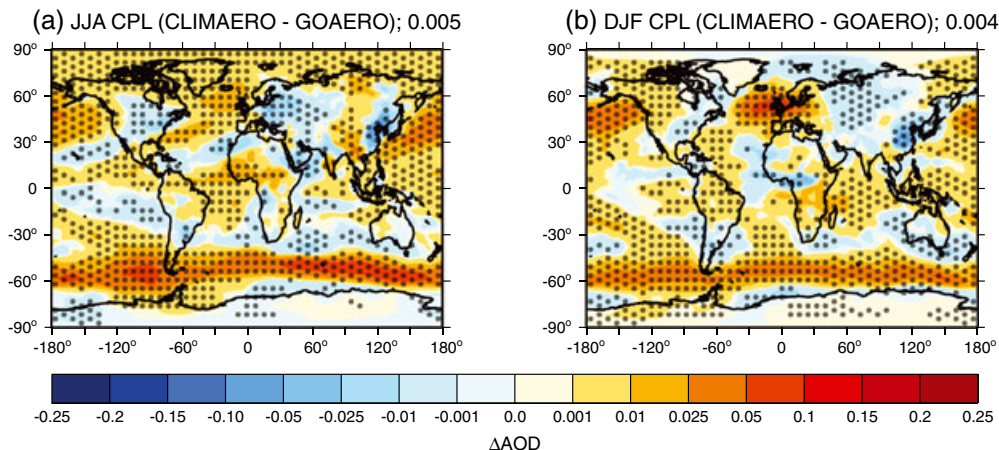


Figure 9. Change in aerosol optical depth (AOD) due to aerosol coupling (CPL or CLIMAERO - GOAERO) in (a) JJA and (b) DJF. Stippling indicates changes significant to 90% confidence. Note: Supplementary Fig. S3 shows the column mass extinction efficiency for the GOAERO ensemble mean (i.e. AOD normalized by the total aerosol column mass loading), and Supplementary Fig. S9 shows the change in column mass extinction efficiency due to aerosol coupling.

variability, however, the mean AOD would be identical in the two model runs except for the sensitivity to relative humidity, which affects the conversion of mass to extinction via the mass extinction efficiency (β_{ext} see Supplementary Material). The virtue of diagnosing the mass extinction efficiency is that it condenses the column variability in aerosol mass distribution and RH into a single quantity and normalizes them by the total mass.

[46] Figure 10 shows the Pearson's correlation coefficient (r) between (a - b) total aerosol AOD and aerosol column mass load (M) and (c - d) column mass extinction efficiency ($\beta_{ext} = AOD/M$) for JJA calculated from daily model output. (See Supplementary Fig. S3 for GOAERO ensemble mean β_{ext} , Fig. S10 for the β_{ext} CPL signal, and S11 for DJF correlations). Statistically significant correlations between AOD and M are generally positive as expected since as aerosol mass increases so does AOD. The correlation between AOD and β_{ext} is generally positive except in regions impacted by dust aerosol (e.g. northern Africa) and in remote regions where there is little aerosol mass (e.g. Antarctica). The negative AOD - mass extinction efficiency correlation over Africa is due to particle size effects. Higher mass loading is associated with larger dust particles, which are less efficient at extinguishing radiation compared to smaller dust particles. Downwind of dust sources, where larger particles are preferentially removed, this negative correlation weakens but remains as column mass loading decreases.

[47] The strongest CPL signal for the change in AOD occurs over the oceans, where AOD is greater in CLIMAERO compared to GOAERO (Fig. 9). From Figure 10, we see that the correlation between AOD and column mass load is more positive over the oceans for GOAERO compared to CLIMAERO, but the correlation between AOD and column mass extinction efficiency is weaker. To illustrate how these relationships impact AOD we examine the sub-monthly variability in aerosol properties (e.g. aerosol emissions, wet deposition, load, optical depth, and mass extinction efficiency) for a single ensemble member from GOAERO (GOAERO E1) and CLIMAERO (CLIMAERO E1) in July (Fig. 11; see Supplementary Fig. S12 for December). We focus on the Southern Ocean (180°W - 180°E , 70°S - 40°S) where sea salt aerosol dominates both AOD (91% of total) and aerosol column mass (92% of total).

[48] For sea salt, which has a very short lifetime (~ 0.87 days; see Supplementary Material), there is a strong positive correlation between wet deposition and emission ($r = 0.85$) and weaker correlations between wet deposition and load ($r = 0.68$) and between emissions and load ($r = 0.53$). GOAERO E1 sea salt AOD has a strong positive correlation with emissions ($r = 0.54$), wet deposition ($r = 0.73$), and column mass loading ($r = 0.82$). There is little correlation between AOD and column mass extinction efficiency for GOAERO E1 ($r = -0.10$), and column mass extinction efficiency and column load are negatively correlated ($r = -0.46$) due to particle size

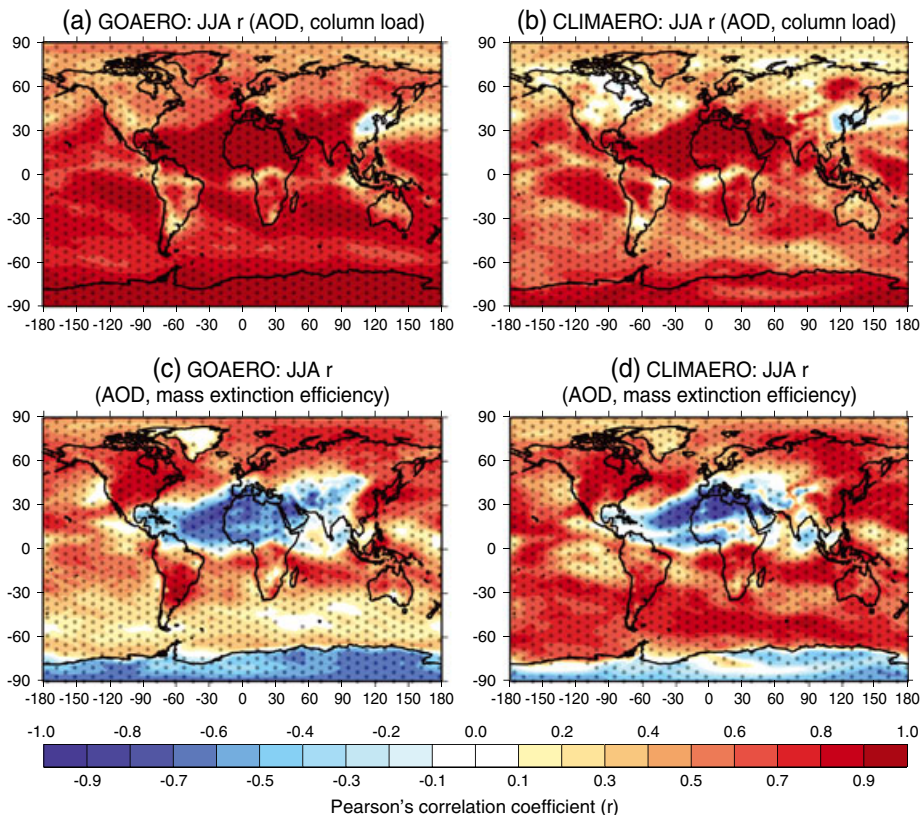


Figure 10. Pearson's correlation coefficient (r) between (a - b) total AOD and aerosol column mass load and (c - d) between total AOD and column mass extinction efficiency (β_{ext}) for interactive (GOAERO) and prescribed (CLIMAERO) aerosols from daily data in JJA (10 years \times 3 months \times ~ 31 days month $^{-1}$ = 930 days for each ensemble mean). Stippling indicates correlations that are significant to 90% confidence based on a two-tailed t-test. See Supplementary Fig. S10 for DJF correlations.

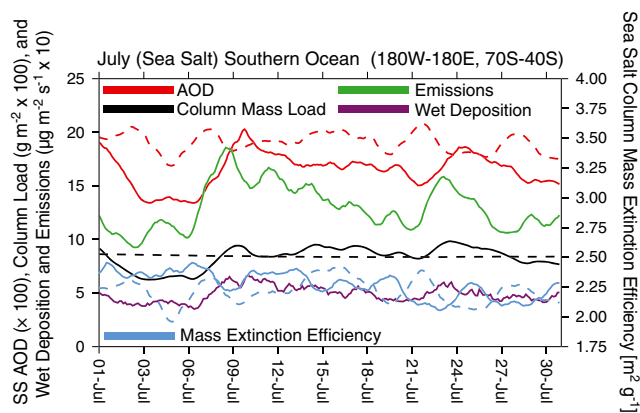


Figure 11. Sub-monthly (3-hour time step) variability in aerosol properties from the first ensemble member of GOAERO (GOAERO E1; solid lines) and the first ensemble member of CLIMAERO (CLIMAERO E1; dashed lines) area-averaged over the Southern Ocean (180°W-180°E, 70°S-40°S) in July (see Supplementary Fig. S11 for December). For sea-salt (SS) aerosol we show AOD (red), column mass load (black), column mass extinction efficiency (blue), emissions (green), and wet deposition (purple). Correlations between these quantities are discussed in the text. The area-averaged change in RH in the Southern Ocean between CLIMAERO E1 and GOAERO E1 is shown in Supplementary Fig. S12.

effects described previously. The correlation between sea salt mass and relative humidity is weak and negative ($r \sim -0.2$ to -0.6) below 700 mb, where the majority of sea salt aerosol mass resides, and correlations are likewise weakly negative between emissions/load/deposition and RH. The weak anti-correlation between loading and relative humidity may be indicative of role of surface dynamics in sea salt generation in the region of the storm tracks, though the exact reason for this anti-correlation remains unclear.

[49] Similar diagnostics (load, AOD and mass extinction efficiency) are presented for the first ensemble member of CLIMAERO in Figure 11 (CLIMAERO E1). The correlation between loading and AOD is negligible ($r=0.04$), because the load is constant across the month. Instead, we find a strong correlation ($r=0.93$) between the AOD and the mass extinction efficiency, which is reflective of the variability in the relative humidity environment of the atmospheric column. The variability (standard deviation as a percentage of the mean) of the mass extinction efficiency is the same for GOAERO E1 and CLIMAERO E1 (5%); however, the variability in sea salt AOD is 10% in GOAERO E1 and 5% in CLIMAERO E1. The mean Southern Ocean July AOD is 15% higher in CLIMAERO E1 compared to GOAERO E1, consistent with the ensemble mean seasonal differences shown in Fig. 9.

[50] The high correlation between AOD and load and the weaker correlation between mass extinction efficiency and loading for GOAERO E1 indicates that the variability in AOD throughout the month is driven to first order by the sub-monthly variability in the loading. In the high-humidity oceanic environment, the AOD is still, however, impacted by changes in the RH environment of the column that amplify the effects of changes in column mass because of the strong sensitivity of mass extinction efficiency to RH.

For CLIMAERO E1, however, the variability in AOD is driven only by variability in RH. The higher AOD in CLIMAERO E1 results from the persistence of constant hygroscopic sea salt mass in the high humidity environment (see Supplementary Fig. S13 for RH changes between CLIMAERO E1 and GOAERO E1).

4. Discussion and Conclusions

[51] We have used the NASA GEOS-5 atmospheric GCM coupled to the GOCART aerosol module to investigate the impact of aerosol-meteorology coupling on the climate response to aerosol (natural and anthropogenic) forcing. We isolate this coupling by considering one set of simulations forced by online, interactive aerosols and another forced by prescribed dry aerosol mass distributions that are consistent with the ensemble mean of the interactive simulations. Results indicate that, relative to a control run with no aerosol forcing, area-average changes in climate are generally of the same sign for both online and prescribed aerosols. The magnitude of these changes may differ significantly, however, for some climate parameters depending on the season and region (e.g. land or ocean). We see the largest differences between prescribed and interactive aerosol forcing near the high latitudes, in the winter hemisphere, and in the stratosphere. These are generally regions remote from the majority of direct aerosol forcing, indicating the likelihood that differing dynamical responses to interactive and prescribed aerosols are occurring. The largest coupling signal is seen for the AOD (and hence aerosol forcing), particularly over the oceans. The lack of sub-monthly variability in aerosol mass combined with changes in relative humidity impacts the aerosol optical depth and forcing such that globally there is additional cooling for prescribed aerosols.

[52] We have tried to understand some of the differences in climate that occur due to coupling by examining the effects of prescribing consistent natural aerosols (dust and sea salt) only. As shown in this study and in previous studies [Randles and Ramaswamy, 2008; Allen and Sherwood, 2011], natural aerosols - which are mostly scattering - tend to drive changes in circulation and temperature that are opposite to the changes imparted by more absorbing anthropogenic and biomass burning aerosols. Further, we see that the impact of prescribed natural aerosols bears strong resemblance to the coupling signal in JJA, indicating that the differences in response between the prescribed and interactive aerosols may be due to differences in natural aerosol forcing, particularly in the southern hemisphere and tropical stratosphere. This is supported by the 3% increase in AOD for prescribed aerosols over the oceans, where sea salt aerosol dominates the aerosol mass.

[53] To further understand the differences in PRE and INT aerosol optical depth and forcing, we examined the sub-monthly variability in aerosol properties for the GOAERO and CLIMAERO ensemble means. We demonstrate that the AOD from short-lived sea salt aerosol is highly correlated with emissions, wet deposition, and loading in GOAERO. In CLIMAERO, because the aerosol mass mixing ratios are fixed for a given month, the correlation between aerosol column mass load and AOD is negligible, but the correlation between AOD and column mass extinction efficiency - which is indicative of the effects of RH changes in the column since

the mass is constant - is high. In the humid oceanic environment, small changes in RH can cause large changes in extinction per unit mass for hygroscopic sea salt aerosol. This amplification effect combined with no sub-monthly variability in aerosol loading result in a higher oceanic AOD in CLIMAERO. Over anthropogenic source regions (e.g. Europe), the burden of anthropogenic aerosols (which have high extinction per unit mass) is less coupled to the meteorological conditions of the model because their emissions are prescribed from monthly-varying inventories. This contrasts with natural aerosols whose burdens are influenced by both emission and loss processes tied to the model meteorology.

[54] Both our PRE and INT signals show strong decreases in high cloud amounts brought on by aerosol effects. Other studies have shown that cloud response is sensitive to the vertical distribution of aerosol heating [e.g. *Takemura and Uchida*, 2011; *Ban-Weiss et al.*, 2012]. A significant heating agent is likely to be black carbon, which has been shown to have its vertical distribution poorly simulated in most modern climate models [*Koch et al.*, 2009]. We did not quantitatively evaluate our simulated black carbon vertical distribution, but qualitatively our distributions are similar to models in *Koch et al.* [2009], showing a generally high black carbon loading at upper levels of the troposphere. As a simple sensitivity study we zeroed out the black carbon loading above 500 hPa in one of our prescribed aerosol runs, likely an extreme overcorrection. Indeed we found the reduction in high cloud amount significantly lessened in this case (i.e., smaller reduction in high cloud amount; see Supplementary Material); however, cloud radiative forcing changes were still consistent with a positive, though weaker, semi-direct effect. An additional experiment to consider would be to reduce the BC burden above 500 mb while preserving the total column loading, which would increase the BC below 500 mb and improve agreement with observed BC vertical profiles (see Supplementary material). Such an experiment is beyond the scope of the current work, but we suggest focusing on the impact of black carbon vertical profile as an important future extension of this work. Owing to the high sensitivity of model response to the vertical distribution of absorbing aerosol, we caution that the response due to aerosol forcing (i.e. INT and PRE) is reflective of the particular aerosol distributions used in the GOAERO and CLIMAERO simulations.

[55] We find some of the strongest changes in temperature and circulation relative to no aerosol forcing in the mid to high-latitudes, and aerosol coupling produces the biggest differences in these regions. The strong high latitude response may partially result from uneven cooling of the land and sea surface when SSTs are fixed. As shown by *Allen and Sherwood* [2011], longer wavelength planetary waves are excited by the land-ocean distribution (and uneven land-ocean aerosol cooling) in the northern hemisphere particularly when SSTs are fixed. These waves are better able to penetrate the stratosphere when SSTs are fixed compared to using a slab ocean model. It may be that much of the CPL signal we observe is due to differences in the planetary wave response that results due to the stronger land surface cooling in the PRE case compared to the INT case.

[56] We have shown that a GCM forced by online, interactive aerosols and one forced by a consistent climatology of dry aerosol mass distributions produces area-average climate

change that are similar in sign. The magnitude of the climate change, however, may be statistically weaker or stronger depending on the parameter, region, or season considered. The strongest coupling signal was on the aerosol optical depth. For the particular model considered in this study, this was due to sub-monthly variability in hygroscopic sea salt burden (or lack thereof) and relative humidity changes. In GEOS-5/GOCART, dust and sea salt emissions and sulfate production from sulfur dioxide gas depend on model meteorology, while all aerosol transport and wet loss depends on the underlying GCM. Aerosol optical properties and thus forcing have a dependence on model RH whether aerosols are prescribed or prognostic. However, while RH varies from time-step to time-step with both interactive and prescribed aerosols, aerosol mass only varies when aerosols are interactive. Removing the co-variability of RH and aerosol mass in the prescribed case has consequences for aerosol optical depth, forcing, and climate response, particularly on a regional basis.

[57] We note that the aerosol-meteorology coupling between GEOS-5 and GOCART is likely representative of a lower-limit compared to more complex prognostic aerosol schemes. Other aerosol schemes - particularly those that have microphysical interactions with clouds - are likely subject to a higher degree of coupling. Therefore it is likely that other GCMs and other prognostic aerosol schemes will exhibit different degrees of the coupling effect examined in this work. Furthermore, the atmospheric forcing in our simulations, as with most GCMs, is weaker than observed [e.g. Table 2 and *Sato et al.*, 2003]. We might expect stronger aerosol impacts from total aerosols with stronger atmospheric absorption, and the coupling effect may change as a result. Our use of fixed SSTs limits the effects of aerosol forcing over the oceans. Atmosphere-ocean feedbacks would likely impact the effects of aerosol-meteorology coupling, particularly because we found our largest differences in aerosol optical depth and forcing over the oceans.

[58] We have highlighted the fact that as models develop more sophisticated treatments of aerosols, it is important to constantly evaluate the impact of these advances on our understanding of aerosol effects on climate. While incorporating prognostic aerosol schemes online in global climate models may enable us to test our understanding of aerosol processes and aerosol-climate interactions, it may not help to reduce uncertainty in aerosol radiative forcing and may complicate our understanding of how the climate responds to such forcing.

[59] **Acknowledgments.** We thank Editor Steve Ghan and three anonymous reviewers for thoughtful comments and suggestions that have helped to improve this manuscript. CAR, PRC, and AMdS acknowledge funding from NASA Modeling Analysis and Prediction (MAP) overseen by David Conidine under project 08-MAP-80. Resources supporting this work were provided by the NASA High-End Computing (HEC) Program through the NASA Advanced Supercomputing (NAS) Division at Ames Research Center and the NASA Center for Climate Simulation (NCCS) at Goddard Space Flight Center under project SMD-11-2567.

References

- Ackerman, A., O. B. Toon, and P. V. Hobbs (1995), A model for particle microphysics, turbulent mixing, and radiative transfer in the stratocumulus-topped marine boundary layer and comparisons with measurements, *J. Atmos. Sci.*, 52, 1204–1236.
- Allen, R. J., S. C. Sherwood, J. R. Norris, and C. S. Zender (2012a), Recent Northern Hemisphere tropical expansion primarily driven by black carbon and tropospheric ozone, *Nature*, 485, 350–354, doi:10.1038/nature11097.

- Allen, R. J., S. C. Sherwood, J. R. Norris, and C. S. Zender (2012b), The equilibrium response to idealized thermal forcings in a comprehensive GCM: Implications for recent tropical expansion, *Atmos. Chem. and Phys. Discussion*, *11*, 31643–31688, doi:10.5194/acpd-11-31643-2011.
- Allen, R. J., and S. C. Sherwood (2011), The impact of natural versus anthropogenic aerosols on atmospheric circulation in the Community Atmosphere Model, *Clim. Dynam.*, *36*, 1959–1978.
- Allen, R. J., and S. C. Sherwood (2010), The aerosol-cloud semi-direct effect and land-sea temperature contrast in a GCM, *Geophys. Res. Lett.*, *37*, L07702, doi:10.1029/2010GL042759.
- Ban-Weiss, G. A., L. Cao, G. Bala, and K. Caldeira (2012), Dependence of climate forcing and response on the altitude of black carbon aerosols, *Clim. Dynam.*, *38*, 897–911, doi:10.1007/s00382-011-1052-y.
- Bauer, S. E., and S. Menon (2012), Aerosol direct, indirect, semi-direct and surface albedo effects from sector contributions based on the IPCC AR5 emissions for pre-industrial and present day conditions. *J. Geophys. Res.*, *117*, D01206, doi:10.1029/2011JD016816.
- Bian, H., P. Colarco, M. Chin, G. Chen, A. R. Douglass, J. M. Rodriguez, Q. Liang, J. Warner, et al. (2012), Investigation of source attributions of pollution to the Western Arctic during the NASA ARCTAS field campaign, *Atmos. Chem. and Phys. Disc.*, doi:10.5194/acpd-12-8823-2012, in press.
- Brioude, J., et al. (2009), Effect of biomass burning on marine stratocumulus clouds off the California coast, *Atmos. Chem. Phys.*, *9*, 8841–8856.
- Charlson, R. J., S. E. Schwartz, J. M. Hales, R. D. Cess, J. A. Coakley, Jr., J. E. Hansen, and D. J. Hofmann (1992), Climate forcing by anthropogenic aerosols, *Science*, *255*, 423–429.
- Chen, G., Y. Ming, N. D. Singer, and J. Lu (2011), Testing the Clausius-Clapeyron constraint on the aerosol-induced changes in mean and extreme precipitation. *Geophys. Res. Lett.*, *38*, L04807, DOI:10.1029/2010GL046435.
- Chin, M., et al. (2002), Atmospheric aerosol optical thickness from the GOCART model and comparisons with satellite and sub photometer measurements, *J. Atmos. Sci.*, *59*, 461–483.
- Chou, M.-D., and M. J. Suarez (1994), An efficient thermal infrared radiation parameterization for use in general circulation models, NASA Tech. Memo, TM-104606, vol. 3, 85 pp.
- Chou, M.-D., and M. J. Suarez (2002), A solar radiation parameterization for atmospheric studies, NASA Tech. Memo, TM-104606, vol. 15, 40 pp.
- Chou, M.-D., M. J. Suarez, X.-A. Liang, and M. M.-H. Yan (2003), A thermal infrared radiation parameterization for atmospheric studies, NASA Tech. Memo, TM-104606, vol. 19, 85 pp.
- Chung, C. E. (2006), Steady vs. fluctuating aerosol radiative forcing in a climate model. *J. Korean. Meteor. Soc.*, *42*(6), 411–417.
- Chung, C. E., and V. Ramanathan (2003), South Asian Haze Forcing: Remote Impacts with Implications to ENSO and AO. *J. Climate*, *16*, 1791–1806.
- Chylek, P., and J. A. Coakley (1974), Aerosols and Climate, *Science*, *183*, 75–77.
- Colarco, P., A. da Silva, M. Chin, and T. Diehl (2010), Online simulations of global aerosol distributions in the NASA GEOS-4 model and comparisons to satellite and ground-based aerosol optical depth, *J. Geophys. Res.*, *115*, D14207, doi:10.1029/2009JD012820.
- Erllick, C., V. Ramaswamy, and L. M. Russell (2006), Differing regional responses to a perturbation in solar cloud absorption in the skyhi general circulation model, *J. Geophys. Res.*, *111*(D6), doi:10.1029/2005JD006491.
- Frierson, D. M. W., J. Lu, and G. Chen (2007), Width of the Hadley cell in simple and comprehensive general circulation models, *Geophys. Res. Lett.*, *34*, L18804, doi:10.1029/2007GL031115.
- Hansen, J., M. Sato, and R. Ruedy (1997), Radiative forcing and climate response, *J. Geophys. Res.*, *103* (D6), 6831–6865.
- Hess, M., P. Koepke, and I. Schult (1998), Optical properties of aerosols and clouds: The software package OPAC. *BAMS*, *79* (5), 831–844.
- Holben, B. N., et al. (1998), AERONET A federated instrument network and data archive for aerosol characterization, *Remote Sens. Environ.*, *66*, 1–16.
- Johnson, B. T., K. P. Shine, and P. M. Forster (2004), The Semi-direct Aerosol Effect: Impact of Absorbing Aerosols on Marine Stratocumulus, *QJRM*, *130* (599), 1407–1422.
- Kang, S. M., L. M. Polvani, J. C. Fyfe, and M. Sigmond (2011), Impact of polar ozone depletion on subtropical precipitation, *Science*, *332*, 951–954.
- Klein, S. A., and D. L. Hartmann (1993), The seasonal cycle of low stratiform clouds. *J. Climate*, *6*, 1587–1606.
- Koch, D., and A. D. del Genio (2010), Black carbon semi-direct effects on cloud cover: review and synthesis, *Atmos. Chem. Phys.*, *10*, 7685–7696.
- Koch, D., et al. (2009), Evaluation of black carbon estimations in global aerosol models. *Atmos. Chem. Phys.*, *9*(22), 9001–9026.
- Koren, I., Y. J. Kaufman, L. A. Remer, and J. V. Martins (2004), Measurement of the effect of Amazon smoke on inhibition of cloud formation, *Science*, 1342–1345.
- Koster, R. D., M. J. Suarez, A. Ducharme, M. Stieglitz, and P. Kumar (2000), A catchment-based approach to modeling land surface processes in a general circulation model 1. Model structure, *J. Geophys. Res.*, *105*, 24,809–24,822.
- Lau, K., M. Kim, and K. Kim (2006), Asian summer monsoon anomalies induced by aerosol direct forcing: The role of the Tibetan plateau, *Clim. Dynam.*, *26*(7–8), 855–864.
- Lesins, G., P. Chylek, and U. Lohmann (2002), A study of internal and external mixing scenarios and its effect on aerosol optical properties and direct radiative forcing, *J. Geophys. Res.*, *107*(D10), doi:10.1029/2001JD000973.
- Liao, H., Y. Zhang, W.-T. Chen, F. Raes, and J. H. Seinfeld (2009), Effect of chemistry-aerosol-climate coupling on predictions of future climate and future levels of tropospheric ozone and aerosols, *J. Geophys. Res.*, *114*, D10306, doi:10.1029/2008JD010984.
- Lin, S.-J. (2004), A vertically Lagrangian finite-volume dynamical core for global models, *Mon. Weather Rev.*, *132* (10), 2293–2307.
- Liu, X., et al. (2011), Toward a minimal representation of aerosols in climate models: description and evaluation in the Community Model CAM5, *Geosci. Model Dev.*, *5*, 709–739, doi:10.5194/gmd-5-709-2012.
- Lock, A. P., A. R. Brown, M. R. Bush, G. M. Martin, and R. N. B. Smith (2000), A new boundary layer mixing scheme. Part I: Scheme description and single-column model tests, *Mon. Weather Rev.*, *128*, 3187–3199.
- Lohmann, U., and J. Feichter (2001), Can the direct and semi-direct aerosol effects compete with the indirect effect on a global scale? *Geophys. Res. Lett.*, *28*(1), 159–161.
- Lu, J., G. Chen, and D. M. W. Frierson (2008), Response of the zonal mean atmospheric circulation to El Niño versus global warming, *J. Climate*, *21*, 5835–5851.
- Menon, S., J. Hansen, L. Nazarenko, and Y. Luo (2002), Climate effects of black carbon aerosols in China and India, *Science*, *297*, 2250–2253.
- Ming, Y., and V. Ramaswamy (2011), A model investigation of aerosol-induced changes in tropical circulation. *J. Climate*, *24*(19), doi:10.1175/2011JCLI4108.1.
- Moorthi, S., and M. J. Suarez (1992), Relaxed Arakawa-Schubert: A parameterization of moist convection for general circulation models, *Mon. Weather Rev.*, *120*, 978–1002.
- Ott, L., B. Duncay, S. Pawson, P. Colarco, M. Chin, C. Randles, and T. Diehl (2010), The influence of the 2006 Indonesian biomass burning aerosols on transport in the tropical UTLS studied with the GEOS-5 AGCM, *J. Geophys. Res.*, doi:10.1029/2009JD013181.
- Pawson, S., R. Stolarski, A. Douglass, P. Newman, J. Nielsen, S. Frith, et al. (2008), Goddard Earth Observing System chemistry-climate model simulations of stratospheric ozone-temperature coupling between 1950 and 2005. *J. Geophys. Res.*, *113*(D12), D12103.
- Perlwitz, J., and R. L. Miller (2010), Cloud cover increase with increasing aerosol absorptivity: A counterexample to the conventional semi-direct aerosol effect. *J. Geophys. Res.*, *115*, D08203, doi:10.1029/2009JD012637.
- Ramanathan V., and G. Carmichael (2008), Global and regional climate changes due to black carbon. *Nat. Geosci.*, *1*, 221–227.
- Ramaswamy, V., et al. (2001), Radiative forcing of climate change, in *Climate Change 2001: The Scientific Basis*, edited by J. T. Houghton et al. pp. 351–406, Cambridge University Press, Cambridge, U. K.
- Randles, C. A., and V. Ramaswamy (2008), Absorbing aerosols over Asia: A Geophysical Fluid Dynamics Laboratory general circulation model sensitivity study of model response to aerosol optical depth and aerosol absorption, *J. Geophys. Res.*, *113* (D21203), doi:10.1029/2008JD010140.
- Randles, C. A., and V. Ramaswamy (2010), Impacts of absorbing biomass burning aerosol on the climate of southern Africa: A Geophysical Fluid Dynamics Laboratory GCM sensitivity study, *Atmos. Chem. Phys.*, *10* (20), 9819–9831.
- Reale, O., K. M. Lau, and A. M. da Silva (2011), Impacts of interactive aerosol on the African Easterly Jet in the NASA GEOS-5 global forecasting system, *Weather Forecast.*, *26*, 504–519, doi:10.1175/WAF-D-10-05025.1.
- Reynolds, R. W., T. M. Smith, C. Liu, D. B. Chelton, K. S. Casey, and M. G. Schlax (2007), Daily high-resolution blended analyses for sea surface temperature, *J. Climate*, *20*, 5473–5496, doi:10.1175/2007JCLI1824.
- Rienecker, M., et al. (2008), The GEOS-5 Data Assimilation System Documentation of Versions 5.0.1, 5.1.0, and 5.2.0, NASA/TM-2007-104606, Vol. 27 (available as pdf at <http://gmao.gsfc.nasa.gov>).
- Rienecker, M., et al. (2011), MERRA - NASA's Modern-Era Retrospective Analysis for Research and Applications, *J. Climate*, *24* (14), 3624–3648.
- Rotstain, L. D. (1997), A physical based scheme for the treatment of stratiform clouds and precipitation in large-scale models. I: Description and evaluation of the microphysical processes. *QJRM*, *123*, 1227–1282.

- Sakaeda, N., R. Wood, and P. J. Rasch (2011), Direct and semidirect aerosol effects of southern African biomass burning aerosol. *J. Geophys. Res.*, *116*, D12205, doi:10.1029/2010JD015540.
- Sato, M., et al. (2003), Global atmospheric black carbon inferred from AERONET, *Proc. Natl. Acad. Sci. U.S.A.*, *100*, 6319–6324.
- Smith, R. N. B. (1990), A scheme for predicting layer clouds and their water content in general circulation models. *QJRM*, *116*, 435–460.
- Solomon, S., D. Qin, M. Manning, M. Marquis, K. Averyt, M. Tignor, H. Miller, and Z. Chen (Eds.), (2007), Technical summary, in *Climate Change 2007: The Physical Science Basis. Contribution of Working Group I to the Fourth Assessment Report of the Intergovernmental Panel on Climate Change*, edited by S. Solomon et al., pp. 19–94, Cambridge Univ. Press, Cambridge, U. K.
- Takemura, T., and T. Uchida (2011), Global climate modeling of regional changes in cloud, precipitation, and radiation budget due to the aerosol semi-direct effect of black carbon, *SOLA*, *7*, 181–184, doi:10.215/sola.2011-046.
- Textor, C., et al. (2006), Analysis and quantification of the diversities of aerosol life cycles within AeroCom, *Atmos. Chem. Phys.*, *6*, 1777–1813.
- Yu, H., et al. (2006), A review of measurement-based assessments of the aerosol direct radiative effect and forcing, *Atmos. Chem. Phys.*, *6*, 613–666.
- Wang, C. (2004), A modeling study on the climate impacts of black carbon aerosols. *J. Geophys. Res.*, *109*, D03106, doi:10.1029/2003JD004084.
- Wilcox, E. M. (2012), Direct and semi-direct radiative forcing of smoke aerosols over clouds. *Atmos. Chem. Phys.*, *12*, 139–149.
- Wilcox, E. M. (2010), Stratocumulus cloud thickening beneath layers of absorbing smoke aerosol. *Atmos. Chem. Phys.*, *10*, 11769–11777, doi:10.5194/acp-10-11769-2010, 2010.
- Wilks, D. S. (2006), *Statistical Methods in the Atmospheric Sciences*, 627 pp., Elsevier Academic Press, Boston, Mass. USA
- Zhang, J., and J. S. Reid (2006), MODIS aerosol product analysis for data assimilation: assessment of over-ocean level 2 aerosol optical thickness retrievals, *J. Geophys. Res.*, *111*, D22207, doi:10.1029/2005JD006898.
- Zhu, Y., and R. Gelaro (2008), Observation sensitivity calculations using the adjoint of the Gridpoint Statistical Interpolation (GSI) analysis system, *Mon. Weather Rev.*, *136*, 335–351, doi:10.1175/MWR3525.